Epiregulin and EGFR interactions are involved in pain processing

Involvement of epiregulin and epidermal growth factor receptor in pain

Loren J. Martin[1,2*], Shad B. Smith[3*], Arkady Khoutorsky[4], Claire A. Magnussen[5], Alexander Samoshkin[7], Robert E. Sorge[1], Chulmin Cho[2], Noosha Yosefpour[5], Sivaani Sivaselvachandran[2], Sarasa Tohyama[2], Tiffany Cole[6], Thang M. Khuong[6], Ellen Mir[3], Dustin G. Gibson[3], Jeffrey S. Wieskopf[1], Susana G. Sotocinal[1], Jean-Sebastien Austin[1], Carolina B. Meloto[7], Joseph H. Gitt[3], Christos Gkogkas[4], Nahum Sonenberg[4], Joel Greenspan[8], Roger B. Fillingim[9], Richard Ohrbach[10], Gary D. Slade[11], Charles Knott[12], Ronald Dubner[8], Andrea G. Nackley[3], Alfredo Ribeiro-da-Silva[5], G. Gregory Neely[6], William Maixner[3], Dmitri V. Zaykin[13], Jeffrey S. Mogil[1*†] and Luda Diatchenko[7*†]

One sentence summary: Epiregulin signals through epidermal growth factor receptor to produce pain.

[1]Dept. of Psychology and Alan Edwards Centre for Research on Pain, McGill University, Montreal, QC H3A 1B1 CANADA

[2]Department of Psychology, University of Toronto Mississauga, Mississauga, ON L5L 1C6 CANADA

[3]Center for Neurosensory Disorders, University of North Carolina, Chapel Hill, NC 27599, USA

[4]Dept. of Biochemistry and Alan Edwards Centre for Research on Pain, McGill University, Montreal, QC H3A 1A3 CANADA

[5]Dept. of Pharmacology and Therapeutics and Alan Edwards Centre for Research on Pain, McGill University, Montreal, QC H3G 1Y6 CANADA

[6]Charles Perkins Centre and School of Life and Environmental Sciences, The University of Sydney, Sydney, NSW 2006 AUSTRALIA

[7]Dept. of Anesthesia, Faculty of Dentistry and Alan Edwards Centre for Research on Pain, McGill University, Montreal, QC H3A 1B1 CANADA

[8]Dept. of Neural and Pain Sciences and Brotman Facial Pain Center,
University of Maryland Dental School, Baltimore, MD U.S.A.

[9]Dept. of Community Dentistry and Behavioral Science, University of Florida,
Gainesville, FL U.S.A.

[10]Dept. of Oral Diagnostic Services, University at Buffalo, Buffalo, NY U.S.A.

[11]Dept. of Dental Ecology, University of North Carolina at Chapel Hill, Chapel Hill, NC U.S.A.

[12]Battelle Memorial Institute, Durham, NC

[13]National Institutes of Environmental Health Sciences, National Institutes of Health,
Research Triangle Park, NC 27709, USA

*These authors contributed equally to the manuscript.

†Co-corresponding authors:

Jeffrey S. Mogil
Dept. of Psychology
McGill University
1205 Dr. Penfield Ave.
Montreal, QC H3A 1B1
CANADA

Luda Diatchenko
Dept. of Anesthesia Research
McGill University
740 Dr. Penfield Ave.
Montreal, QC H3A 0G1
CANADA

ABSTRACT

The epidermal growth factor receptor (EGFR) belongs to the well-studied ErbB family of receptor tyrosine kinases. EGFR is activated by numerous endogenous ligands that promote cellular growth, proliferation and tissue regeneration. In the present study, we demonstrate a novel function for EGFR and its natural ligand, epiregulin (EREG), in pain processing. We show that inhibition of EGFR with clinically used compounds strongly reduces nocifensive behavior in mouse models of inflammatory and chronic pain. EREG enhances nociception through a mechanism that involves the PI3K/AKT/mTOR pathway and matrix metalloproteinase-9. In sensory neurons, EREG potentiates the calcium influx induced by the TRPV1 agonist, capsaicin, but not the TRPA1 agonist, mustard oil. Both the *EGFR* and *EREG* genes display genetic association with the development of chronic pain in several clinical cohorts of temporomandibular disorder. Thus, EGFR and EREG may be suitable therapeutic targets for persistent pain conditions.

INTRODUCTION

Chronic pain is a major human health problem affecting almost one-quarter of the population at any one time (1-3). Chronic pain is difficult to manage and treatment options are limited and associated with unwanted side effects, and the identification of novel pharmacotherapeutic targets remains challenging. Recently, the epidermal growth factor receptor (EGFR) has received attention for its therapeutic potential. EGFR inhibition is the first-line treatment for non-small cell lung cancer, and there have been a number of case reports suggesting that EGFR inhibition provides rapid relief of cancer pain (4-8). Cancer patients administered EGFR inhibitors report a significant reduction in pain scores and an overall improvement in quality of life without an obvious effect on tumor progression and size (6).

EGFR is a member of the ErbB family of tyrosine kinase receptors (9) that regulate cellular growth, survival, proliferation and differentiation of fibroblasts and hepatocytes (10, 11). Several ligands can bind to and activate EGFR, including EGF, transforming growth factor α (TGF- α), heparin-binding EGF-like growth factor (HB-EGF), amphiregulin, betacellulin, and epiregulin (EREG) (9). The downstream effects of EGFR are mediated by a number of important signaling pathways, including mitogen-activated protein kinase (MAPK) (8) and PI3K/AKT/mammalian target of rapamycin (mTOR)—which are known to regulate pain (12-14). EGFR has been shown to affect receptors important for pain processing, including opioid receptors (15), β-adrenergic receptors (16) and cannabinoid type 1 (CB1) and transient receptor potential cation channel, subfamily V, member 1 (TRPV1) receptors (17). However, none of these previous reports examined these interactions using behavioral or cellular models specifically relevant to pain processing. Here, our primary goal was to understand the EGFR pathway's role and mechanism of action in pain processing.

We investigated the role of the EGFR and its ligands in nociception using murine behavioral and *ex vivo* studies to identify mechanistic targets for EGFR signaling in pain that may be generalizable across pain conditions. Specifically, we demonstrate herein that inhibition of the tyrosine kinase site of the EGFR, using both experimental and clinically available compounds, is analgesic against a variety of tonic and chronic pain modalities in the mouse. The genes coding for both EGFR and EREG demonstrate genetic association with a human chronic pain syndrome, temporomandibular disorder, and genetic inhibition of EGFR modulates pain behavior in both mice and *Drosophila*. Finally, we show that stimulation of EGFR, by its ligand EREG specifically, activates DRG neurons, producing pain behaviors through a mechanism that involves TRPV1, the PI3K/AKT/mTOR/4E-BP1 signaling pathway, and matrix metalloprotease-9 (MMP-9), a molecule known to be involved in inflammation and the early stages of chronic pain (18).

RESULTS

Modulation of EGFR affects pain sensitivity in mice

To assess the effect of EGFR inhibition on pain in mice we tested one preclinical (tyrphostin AG 1478; hereinafter, AG 1478; 10 mg/kg) and two clinically available (50 mg/kg gefitinib and 75 mg/kg lapatinib) EGFR tyrosine kinase inhibitors in a battery of algesiometric assays. Doses were chosen based on prior in vivo efficacy against stress-induced necrotic lesions in the heart (AG 1478), and chemoprevention of lung cancer (gefitinib) or breast cancer (lapatinib) in mice (19-21). We first confirmed that none of the drugs, delivered systemically and at very high doses (AG 1478, 100 mg/kg; gefitinib, 300 mg/kg; lapatinib, 300 mg/kg) produced significant ataxia over a 1-h testing period on the rotarod test (Figure 1A). These drugs did not affect acute noxious thermal (Figure 1B) or mechanical (Figure 1C) sensitivity. By contrast, in the formalin test EGFR inhibitors produced robust inhibition of tonic inflammatory pain (Figure 1D), without affecting edema (not shown). Compilation of full dose-response curves revealed dose-dependent analgesia only in the late or tonic phase (Figure 1E), with efficacy and potencies comparable to morphine (see Supplemental Table 1). Further, EGFR inhibition completely reversed the thermal hypersensitivity produced by an inflammatory mediator, λ-carrageenan, at 20-40 min post-injection (Figure 1F). Finally, we examined mechanical hypersensitivity (allodynia) after longer-lasting inflammatory and neuropathic injuries. Higher doses were required, but all drugs produced complete and dose-dependent reversal of allodynia in complete Freund's adjuvant (CFA) model of inflammatory pain (Figure 1G). Similarly, all drugs produced complete and dose-dependent reversal of allodynia in the spared nerve injury (SNI) model of neuropathic pain (Figure 1H). Half-maximal analgesic doses and confidence intervals for the EGFR inhibitors for

CFA and SNI are presented in Supplemental Table 2. In a separate experiment we used the chronic constriction nerve injury (CCI) model of chronic pain to provide generalizability across neuropathic assays. Similar to SNI, EGFR inhibition produced robust anti-allodynia on CCI (Figure 1I).

Activation of EGFR by EREG, but not other EGFR ligands, promotes nociception

In order to determine whether EGFR activation is sufficient to increase nociception, we screened a number of EGFR ligands for their ability to promote nocifensive behaviors in the formalin test. We find that late phase formalin-induced nocifensive behaviors were enhanced in a dose-dependent manner with intrathecal (i.t.) injections of EREG, but none of the other tested EGFR ligands including betacellulin, TGF-α, amphiregulin or epidermal growth factor (EGF) (Figure 2A). EREG produced a robust and dose-dependent increase in licking behavior that was indistinguishable from that produced by nerve growth factor (NGF), known for its prominent role in pain processing (Figure 2A). Next, we assessed whether EREG enhanced pain behaviors induced by capsaicin or mustard oil, two potent algogens known to activate TRPV1 and TRPA1, respectively. Intrathecal delivery of EREG potentiated nocifensive behavior from intraplantar capsaicin but not mustard oil (Figure 2B). In addition, the TRPV1 antagonist, AMG 9810 (30 mg/kg; i.p.), but not the TRPA1 antagonist, HC-030031 (30 mg/kg; i.p.) blocked the hyperalgesic effect of EREG on the late phase of the formalin test (Figure 2C). Spinal delivery of EREG produced both thermal (Figure 2D) and mechanical (Figure 2E) pain hypersensitivity in the absence of injury. EREG's hyperalgesic effects on the formalin test were independent from other tyrosine receptor kinases, as K252a (an inhibitor of TrkA, TrkB and TrkC) but not EGFR failed to block EREG-induced hypersensitivity (Supplemental Figure 1). Furthermore, administration of

AG 1478 blocked the hyperalgesic effects of EREG on the formalin test, but did not reverse the hyperalgesia produced by intrathecal injections of NGF, a potent activator of TrkA, confirming that EREG-mediated hypersensitivity is dependent on the EGFR and not TrkA (Supplemental Figure 1).

EGFR gene mutant effects in mice and *Drosophila*

In order to confirm the efficacy of EREG in promoting pain hypersensitivity, we tested a partial loss of function EGFR mutant mouse for EREG-induced hypersensitivity. The EGFRvIII/ΔEGFR mutant mouse has a large deletion of the extracellular domain that renders EGFR constitutively active but with no ability to bind extracellular ligands (22). The homozygous mutation is embryonically lethal, and thus we tested ΔEGFR heterozygotes for EREG-induced pain sensitivity on the formalin test. Basal formalin-induced licking behavior of ΔEGFR heterozygotes was increased, but EREG no longer produced hypersensitivity on the formalin test (Figure 2F). The increased formalin sensitivity of ΔEGFR heterozygotes was likely due to constitutive activity of the EGFR. Since further activation by ligand binding is reduced in this mutant, EREG would not be expected to increase pain behavior any further. In addition, we used genetic knockdown and somatic *Drosophila* mutants to confirm that EGFR acts via sensory neurons to mediate nociception in response to a 46 °C probe (Supplemental Figure 2). The *Drosophila* data establish that the EGFR system is a conserved component of the nociceptive processing apparatus.

EGFR is conserved from humans through to the fruit fly *Drosophila melanogaster* (23). Since fruit fly larvae exhibit robust nociceptive behavior in response to noxious heat (24), we next tested if EGFR also regulates nociception in insects. Animals with *Egfr* knocked down in peripheral *ppk*+ nociceptor neurons exhibit impaired thermal nociception (Supplemental Figure 2, A–C), and

conversely reintroduction of intact *Egfr* specifically in *ppk*+ sensory neurons was sufficient to rescue nociception in whole body *Egfr* somatic mutant animals (Supplemental Figure 2, D–F). Together, these data establish that the EGFR system is a conserved component of the nociception apparatus, regulating peripheral nociceptor function *in vivo*.

EREG and _EGFR_ genetic loci are associated with the risk of development of a chronic pain condition

Since our studies in mice indicate a robust role for EREG and EGFR in mediating pain, we next searched for evidence that EGFR contributes to pain in a human clinical population. Three human cohorts of a common chronic pain condition, temporomandibular disorder (TMD), were assessed in four case-control association analyses (Supplementary Table 3) on a panel of 358 pain-relevant candidate genes. In the first analysis, designed to minimize experimental variance, we contrasted 127 Caucasian female TMD cases from the OPPERA (Orofacial Pain: Prospective Evaluation and Risk Assessment) (25) cohort against a subset of 231 demographically matched "super-controls," who reported absolutely no procedural pain at exam. Of the genes screened, *EREG* (rs1563826, odds ratio = 0.4, p=2.0 x 10^{-4}) (Figure 3A), and *EGFR* (rs1140475, odds ratio = 2.6, p=2.2 x 10^{-4}) (Figure 3B) demonstrated the highest association with the development of TMD. In addition, the majority of SNPs deviating from the QQ plot were located in either *EREG* or *EGFR* loci (Supplemental Figure 3A). Formal pathway analysis identified the EGFR signaling pathway as significantly associated with TMD (p=0.0013; Supplemental Table 4). Nominally significant (p<0.05) associations were also observed for *EREG* and *EGFR* in the full OPPERA cohort, in which TMD cases were contrasted with all 731 enrolled TMD-free controls (Figure 3, A and B). We replicated these association results in two independent cohorts of Caucasian females, including

one case-control study of 200 TMD cases and 198 controls ("TMD case-control cohort") (26), and another prospective study of 186 initially pain-free subjects in which 15 developed TMD over a three-year follow-up period ("pre-OPPERA cohort") (27). These analyses identified several additional single nucleotide polymorphisms (SNPs) with either significant or borderline associations (Figure 3, A and B). Whereas the pattern of association within the *EREG* gene locus was identical in all four cohorts (Figure 3A), with SNP rs1563826 showing the strongest association with TMD, the pattern of association for *EGFR* differed between cohorts (Figure 3B). To explain the discrepancies in single SNP results between cohorts, the *EGFR* gene locus was subjected to haplotype analysis that produced convergent results (Supplemental Table 5).

Total RNA isolated from blood leukocytes was collected from participants of the TMD case-control study. Relatively high expression levels of *EREG* (but not *EGFR*) in leukocytes allowed us to measure *EREG* mRNA using quantitative PCR (qPCR) in all subjects, and evaluate its association with *EREG* genotypes. The minor allele T of SNP rs1563826, which showed the strongest association with decreased odds of TMD (Figure 3C), was also associated with lower *EREG* mRNA levels (Figure 3D), suggesting that higher levels of EREG contributes to hyperalgesic states in patients.

We then assessed the *EREG* gene locus for functional SNPs potentially responsible for transcript regulation. No SNPs with minor allele frequency >5% are reported within 5 kB upstream of the *EREG* promoter. However, the synonymous rs2367707 SNP within the *EREG* coding region was found to be in close-to-perfect linkage disequilibrium with rs1563826, and with an almost identical *p*-value of TMD risk (Figure 3A). To examine the effect of rs2367707 allelic variants on transcript levels, we transfected HEK293 cells with expression constructs that carried allelic variants of rs2367707. In line with the genetic effect of the *EREG* haplotype on endogenous mRNA

levels, the minor A allelic variant of *EREG* showed significantly lower transcript stability than the major G allelic variant (Figure 3E). The association of *EGFR* and *EREG* with chronic pain in a clinical cohort is a significant translational complement to our mouse data, and supports the potential value of targeting EGFR for chronic non-cancer pain management in humans.

EREG levels and EGFR phosphorylation are upregulated in mouse models of chronic pain

The finding of increased *EREG* mRNA levels in leukocytes of TMD patients (Figure 3D) prompted us to investigate whether chronic pain states in mice are associated with increased levels of EREG in the blood. CFA and SNI (but not formalin) produced a massive upregulation of EREG, as assessed by ELISA (Figure 4A). To study the site of EREG action we investigated the distribution of EGFR in DRGs and spinal cord. EGFR was non-homogeneously expressed by all DRG neurons within the cytoplasm of individual DRG cells, and neuronal size did not affect EGFR expression levels (Figure 4, B and C). In the spinal cord, EGFR expression was very low and was not found on neurons (Supplemental Figure 4). Immunostaining of EREG was not possible due to lack of appropriate antibodies. Based on our findings of increased EREG levels in CFA and SNI, we hypothesized that the activity of the EGFR should be increased in these conditions. To this end, we measured the phosphorylation of EGFR (on Tyr1068), which is reflective of EGFR activation, in lysates prepared from mouse DRG. EGFR phosphorylation was significantly increased following CFA and SNI (Figure 4, D and E), consistent with the hypothesis that chronic inflammatory and neuropathic injury-induced increases in EREG levels enhances EGFR phosphorylation. Since EREG potentiated capsaicin-dependent nocifensive behavior, we next measured whether EREG (200 ng/ml) potentiates TRPV1-dependent calcium transients in cultured DRG neurons. EREG caused a robust increase of calcium responses after a single application of

capsaicin (1 μM) but not mustard oil (100 nM), confirming at the cellular level that EREG potentiates TRPV1 but not TRPA1 responses (Figure 4, F and G; see also Supplemental Figure 5).

EREG pain hypersensitivity is mediated by a signal transduction pathway involving mTOR, translational regulation, and MMP-9

Since our preclinical and clinical data indicated a critical role of EREG (but not other EGFR ligands) and EGFR in pain processing, we sought to determine the intracellular machinery by which EREG-mediated EGFR activation increases pain. EGFR signaling has previously been shown to increase the activity of mTOR (28), a master regulator of mRNA translation (29, 30). Therefore, we hypothesized that mTOR is a downstream effector of EGFR with respect to pain. We investigated the contribution of mTOR signaling to EREG-induced hypersensitivity by screening nocifensive behaviors on the formalin test and disrupting elements of the mTOR signal transduction pathway, either with pharmacological inhibitors or, where available, using null mutants (See Figure 5A for an overview of the pathway). Pretreatment with wortmannin, a covalent inhibitor of phosphoinositide 3'-kinase (PI3K), completely abolished EREG-induced hypersensitivity without affecting formalin-induced pain behavior *per se* (Figure 5B). Next, we tested two inhibitors of mTOR, rapamycin and CCI 779. At higher doses, these drugs produced analgesia on the formalin test, as has been reported previously (29, 30). However, at lower doses, both drugs prevented EREG-induced hypersensitivity without affecting formalin-induced pain behavior *per se* (Figure 5C). mTOR regulates mRNA translation via two downstream effectors: ribosomal protein S6 kinases (S6Ks) and eukaryotic translation initiation factor 4E (eIF4E)-binding protein 1 (4E-BP1). Mutant mice lacking expression of both S6K 1 and S6K 2 (S6K1/2 double knockout) showed completely intact EREG-induced hypersensitivity (Figure 5D),

whereas 4E-BP1-deficient mice displayed no EREG-induced hypersensitivity (Figure 5E). 4E-BP1 represses the formation of the eukaryotic translation initiation factor F (eIF4F) complex, which is a critical regulator of cap-dependent translation. An inhibitor of eIF4F complex, 4EGI-1, blocked EREG-induced hypersensitivity (Figure 5F), further supporting the role of mTOR/4E-BP1/eIF4F in pain. To determine whether EREG hypersensitivity was mediated in part by ERK signaling, we used the MEK1/MEK2 inhibitor PD98059 (31). A low concentration of PD98059 did not block EREG-induced hypersensitivity on either the formalin test or the von Frey test (Supplemental Figure 6), suggesting that EREG does not potentiate pain behavior through enhanced ERK signaling. Since enhanced eIF4F complex formation has been shown to increase endogenous metalloproteinase-9 (MMP-9) in blood (32), we used tissue inhibitor of metalloproteinases-1 (TIMP-1), an endogenous blocker of MMP-9, and *Mmp9*$^{-/-}$ mice to study whether MMP-9 signaling is important for EREG-induced pain hypersensitivity. TIMP-1 prevented (Figure 5G, also see Supplemental Figure 7A) and *Mmp9*-/- mice did not display EREG-induced hypersensitivity (Figure 5H). We further tested the importance of MMP-9 for EGFR pain signaling by confirming that the analgesic efficacy of gefitinib in the formalin test was abolished in *Mmp9* $^{-/-}$ mice (Supplemental Figure 7B).

To further study the role of mTOR and MMP-9 in EGFR-mediated pain, we examined the phosphorylation of mTOR pathway components in DRG lysates. Formalin treatment alone did not significantly increase the phosphorylation of AKT (p-AKT), but EREG increased p-AKT in DRG tissue relative to control (Figure 6, A and B). Congruent with our behavioral data, both formalin and EREG increased the phosphorylation of 4E-BP1 (p-4E-BP1) in DRG tissue, and co-treatment with rapamycin prevented this increase (Figure 6, A and C). Further, p-S6 was significantly increased with EREG treatment, and again, co-treatment with rapamycin prevented the increases

(Figure 6, A and D). Finally, MMP-9 protein levels were increased in DRG tissue after formalin or EREG injection, and this increase was blocked with rapamycin inhibition of mTOR (Figure 6, A and E).

To determine whether the increase in MMP-9 protein levels following EREG treatment was the result of increased *Mmp9* mRNA translation, DRG extracts were fractionated on sucrose density gradients, and the distribution of *Mmp9* mRNA across these gradients was determined by qPCR analysis. In DRG extracts, *Mmp9* mRNA shifted to the heavy polysome fractions after EREG injection, indicative of enhanced translation (Supplemental Figure 8). Rapamycin blocked this shift, indicating that in the DRG, EREG stimulates *Mmp9* mRNA translation in an mTOR-dependent manner. Taken together our results support a key role for mTOR, the eIF4F translational initiation complex, and MMP-9 signaling in EGFR-mediated pain behavior.

DISCUSSION

Although there are indications from the clinical literature that EGFR inhibition may have analgesic properties (5, 6, 8), this possibility has not heretofore been examined systematically. Here, we used a broad range of techniques and data analyses to demonstrate that: 1) EGFR inhibition is analgesic and activation of the EGFR by EREG enhances pain; 2) EREG and EGFR display a genetic association with the development of chronic pain in clinical cohorts of temporomandibular disorder; and 3) EREG increases pain behavior and signaling through a mechanism that involves TRPV1 and mTOR/eIF4F/MMP-9-dependent signaling in the DRG.

We find that the EGFR is expressed by all DRG sensory neurons (Figure 4, B and C), and show that EREG potentiates capsaicin-induced calcium influx, suggesting that functional EREG receptors are present in DRG neurons (Figure 4F and G). In addition, we provide compelling evidence that EREG increases pain sensitivity through EGFRs, whereas other EGFR ligands do not appear to play a role. This is consistent with prior observations that EGF or the heparin-bound EGF do not increase sensitivity to painful stimuli (33). EGF-like growth factors, including EREG, stimulate a variety of biological responses, and it is thought that ligand-induced homo- and heterodimerization can account for the majority of this diversity (34, 35). For instance, EREG is known to bind to and phosphorylate heterodimers of EGFR and ErbB-4, but other EGF ligands (i.e. EGF and amphiregulin) only activate EGFR homodimers (36, 37). We suspect that an associated membrane protein, such as ErbB4 is involved in EREG-induced hypersensitivity, but this currently remains unclear.

Our human data further support a role of EREG in pain as we find that *EREG* was associated with TMD development and upregulated in the blood of the patients. Moreover, our genetic

association results revealed a strong effect of genetic polymorphism in the EREG–EGFR system distinguishing those with chronic pain from controls. The observed association between TMD risk, *EREG* mRNA level and transcript stability, suggests that rs2367707 may be the functional SNP in humans. The fact that the TMD protective allele is associated with lower mRNA expression is congruent with our rodent findings. The *EGFR* SNPs tested in this study are probably only markers of the true effect-producing variants, but both 5'- and 3'-located SNPs within the *EGFR* locus showed association signals, suggesting both expression differences and transcript stability, respectively, may alter TMD risk. Thus, our results suggest that targeting EGFR and EREG for pain therapies may be an effective strategy. Importantly, since EGFR inhibition is associated with adverse side effects—folliculitis, hair loss and skin rash—inhibition of EREG may constitute an improved therapeutic option for pain management.

At the cellular level, the effects of EREG on EGFR involve TRPV1, as co-application of capsaicin enhanced EREG-induced activation of sensory neurons, and blockade of TRPV1 attenuated EREG hyperalgesia in the formalin assay. TRPV1 has been shown to induce EGFR transactivation in a model of epithelial wound healing, leading to PI3K/AKT stimulation (17). This is in line with our current findings that showed disruption of PI3K/AKT/mTOR signalling with specific inhibitors of the AKT/mTOR pathway blocked, and 4E-BP1 null mice lacked, EREG-induced hypersensitivity. In the DRG, EREG or formalin increased the phosphorylation of both S6 and 4E-BP1, the two main downstream targets of mTOR. However, since S6K1/2 null mutant mice had intact EREG-induced hypersensitivity we conclude that S6K is not necessary for EREG-stimulated pain behavior. In addition, our results indicate that EREG-induced pain behavior is not mediated by ERK signalling, an observation that is consistent with data showing that EREG does not activate ERK in DRG neurons (33). Further, our data indicate that the phosphorylation of

4E-BP1 increases the translation of MMP-9, and pharmacological or genetic reduction of MMP-9 activity renders EREG and EGFR antagonists ineffective against inflammatory pain. Together, our results indicate that EREG upregulation in the blood may activate EGFRs on DRG neurons to induce hypersensitivity through transactivation of TRPV1 and the mTOR signaling pathway, which increases MMP-9 translation. It is likely that EREG is originating from the blood as we find elevated levels of EREG following CFA and SNI, which parallel EREG mRNA expression levels in TMD patients.

In summary, we find that clinically available small molecule EGFR inhibitors targeting the tyrosine kinase site of the EGFR receptor, including gefitinib and lapatinib, are effective analgesics in mice, for inflammatory and neuropathic pain. These drugs are routinely given to non-small-cell lung cancer patients (38, 39) to inhibit tumor growth, but have not been systematically studied for their role in pain management. Since we find that EREG is the primary endogenous activator of EGFR-related pain hypersensitivity, our data suggest that an effective treatment strategy may be the selective inhibition of EREG over other endogenous EGFR ligands. Directly targeting EREG may result in a reduced side-effect profile when compared with currently available EGFR-inhibition strategies.

METHODS

Study design

Animals were randomized to drug condition using within-cage randomization, and all behavioral experiments were performed by an experimenter blinded to drug conditions. As we had no *a priori* expectation of effect sizes, power analyses were not used to calculate sample sizes. Instead, we adhered to standard practices in the field (38). In many cases, sample sizes were dictated by breeding success. Statistical outliers were defined via Studentized residuals >3, and excluded before analyses were run.

Rodent subjects

Most experiments were performed on naive, adult (7–12 weeks of age) outbred CD-1® (ICR:Crl) mice of both sexes, bred in-house (J.S.M. laboratory) from breeders obtained from Charles River (Boucherville, QC). Heterozygote breeding pairs for mutant mice containing a large deletion of the extracellular domain of the EGFR receptor (EGFRvIII/ΔEGFR) were obtained from the laboratory of Dr. David Threadgill (North Carolina State University) on a C57BL/6 background. We only tested heterozygote EGFRvIII/ΔEGFR mice because the homozygotes are neonatally lethal. Null mutant mice for 4E-BP1 (*Eif4ebp*-/-; C57BL/6 background) and p70 S6 kinase 1/2 double knockout mice (*Rps6kb1/Rps6kb2* -/-; mixed 129Sv x C57BL/6 background) and their associated wildtypes were generated and bred in one of our laboratories (N.S.). The latter mutants were kindly provided by Dr. G. Thomas (University of Cincinnati). Mice lacking the MMP-9 gene (*Mmp9* -/-) were purchased from The Jackson Laboratory on an FVB/NJ background and compared to wildtype mice of that strain. No overt behavioral abnormalities were noted in any of the mutant mouse strains. All mice were housed with their same-sex littermates (two to four

animals per cage) in standard shoebox cages, maintained in a temperature-controlled (20 ± 1 °C) environment (14:10 h light/dark cycle), and fed (Harlan Teklad 8604) and watered *ad libitum*. Mice were assigned to experimental conditions in a randomized fashion within-cage.

All procedures were approved by the local animal care and use committees at McGill University and the University of Toronto Mississauga and were consistent with national guidelines.

Behavioral assays

Subjects were habituated to the testing environment for at least 15 min in every assay before testing commenced. Animals were randomized to drug condition, and all behavioral experiments were performed by an experimenter blinded to conditions.

Rotarod test: Drug effects on motor coordination were tested using an accelerating rotarod treadmill (Acceler Rota-Rod 7650, UgoBasile) for mice (40). Mice were placed on the rotarod, which accelerated from 4 to 40 rpm over a period of 5 min, and the time spent on the rotating drum was recorded for each mouse. On the test day, one pre-injection baseline trial (drug-free) was performed before the animals were treated with either saline, AG 1478 (100 mg/kg), gefitinib (300 mg/kg) or lapatinib (300 mg/kg). Performance was indicated by the latency to fall from the rotarod at 15–60 min after injection.

Radiant heat paw-withdrawal test: Mice were placed on a 3/16th-inch thick glass floor within small Plexiglas cubicles (9 × 5 × 5 cm high), and a focused high-intensity projector lamp beam was shone from below onto the mid-plantar surface of the hind paw (41). The commercial device (IITC Model 336) was set to 20% active intensity. Latency to withdraw from the stimulus was measured to the nearest 0.1 s. Baseline measurements consisted of testing both hind paws twice

on three separate occasions separated by at least 30 min. Following drug injection, both hind paws were only tested once at the indicated time.

von Frey test: The up-down method of Dixon (42) was used. Mice were placed on a perforated metal floor (with 5-mm diameter holes placed 7 mm apart) within small Plexiglas cubicles as described above, and a set of eight calibrated von Frey fibers (Stoelting Touch Test Sensory Evaluator Kit #2 to #9; ranging from ≈0.015 g to ≈1.3 g of force) were applied to the plantar surface of the hind paw until the fibers bowed, and then held for 3 s. The threshold force required to elicit withdrawal of the paw (median 50% withdrawal) was determined twice on each hind paw (and averaged) for all baseline measurements, with sequential measurements separated by at least 20 min. For experiments in which a drug was injected, one measurement per hind paw was taken at the indicated time point.

Formalin test: Formalin injection produces a biphasic response: an acute, nociceptive "early" phase and a tonic, inflammatory "late" phase, separated by a quiescent period in which there is no apparent pain behavior (41). Mice were placed on a tabletop within Plexiglas cylinders (30 cm high; 30 cm diameter) and allowed to habituate. Then, 20 µl of 5% formalin was injected subcutaneously into the plantar surface of the left hind paw using a 100-µl microsyringe with a 30-gauge needle. Mice were then returned to the cylinders, and left undisturbed for 60 min, with behaviors recorded using digital video. Videos were later coded offline, where the first 10 s of every minute was monitored for the presence of licking/biting (positive sample) of the left hind paw for a total of 60 observations. The early phase was defined as the percentage of positive samples during the first 0–10 min post-injection of formalin; the late phase as the percentage of positive samples during the period 10–60 min post-injection. For the drug studies, EGFR, TRPV1, TRPA1 and mTOR inhibitors were injected 20 min before formalin, and TIMP-1 was injected 1 h

before formalin. EGFR ligands and NGF were injected immediately before formalin.

Carrageenan: Carrageenan (2%; 20 mg/ml; Sigma) was suspended by sonication in saline, and injected subcutaneously in a volume of 20 µl into the left plantar hind paw using a 100-µl microsyringe with a 30-gauge needle. Mice were tested for thermal sensitivity of both hind paws using the radiant heat paw withdrawal test as described above, before and 3 h post-carrageenan injection. All drugs were injected immediately following the test for carrageenan hypersensitivity at the 3 h time point, and post-drug measurements were taken at 20, 40 and 60 min.

Complete Freund's adjuvant: Complete Freund's adjuvant (CFA; 50%; Sigma) was injected subcutaneously in a volume of 20 µl into the left plantar hind paw using a 100-µl microsyringe with a 30-gauge needle. Mice were tested for mechanical sensitivity of both hind paws using the von Frey test as described above, before and 3 days post-CFA injection. All drugs were injected immediately following the 3 day post-CFA test, and post-drug measurements were taken at 20, 40, 60 and 90 min. Percentage of maximal possible anti-allodynia (i.e., reversal of allodynia back to pre-injection baseline values at all post-drug time points) was calculated using the trapezoidal method.

Spared nerve and chronic constriction injury: Spared nerve injury (SNI) and chronic constriction injury (CCI), two experimental nerve injury procedures designed to produce neuropathic pain, were performed under isoflurane/oxygen anaesthesia as described previously (43, 44). Mice were tested for mechanical sensitivity before and after surgery using the von Frey test as described above, except that the "spared" sural region was targeted for SNI and the mid-plantar surface was targeted for CCI by applying the fibers to the hind paw. All drugs were injected immediately following the test for SNI- or CCI-induced mechanical allodynia 7 or 14 days following surgery, respectively, and post-drug measurements were taken at 20, 40, 60 and 90 min.

Percentage of maximal possible anti-allodynia (i.e., reversal of allodynia back to pre-surgery baseline values at all post-drug time points) was calculated using the trapezoidal method.

Capsaicin and mustard oil: Mice were allowed to habituate to an observation chamber (see formalin test above) for 15 min. Mice then received a subcutaneous injection of capsaicin (2.5 μg; Sigma) or mustard oil (5%; Sigma) into the plantar left hindpaw (20 μl) and were digitally videotaped for 10 min. Video files were later scored for the total duration (s) of licking/biting of the injected paw.

Drugs

AG 1478, gefitinib, lapatinib, rapamycin, CCI 779 and wortmannin were purchased from LC Laboratories (Woburn, MA) and dissolved in 30% polyethylene glycol except wortmannin, which was dissolved in 10% DMSO. EREG, EGF, betacellulin, amphiregulin, TGF-α, NGF, AMG 9810, K252a, PD 98059 and TIMP-1 were purchased from R&D Systems (Minneapolis, MN) and were dissolved in sterile saline, except K252a and PD 98059, which were dissolved in 20% DMSO. Capsaicin, Mustard Oil and HC 030031 were purchased from Sigma Aldrich (Mississauga, ON). 4EGI-1 was purchased from Santa Cruz Biotechnology (Santa Cruz, CA) and dissolved in 20% DMSO. Morphine sulfate was obtained from Health Canada and dissolved in saline. Drugs were administered either intraperitoneally (10 ml/kg volume) or intrathecally (5 μl volume) (45).

Enzyme-linked immunosorbant assay

Mice received no treatment, formalin injection, CFA injection, or SNI surgery, and were euthanized 60 min (formalin), 3 days (CFA), or 7 days (SNI) later. Trunk blood was collected into EDTA-coated Vacutainer tubes/heparinized syringes. Blood was centrifuged at 15,000 rpm for 15

min at 4 °C to isolate plasma from other blood components. Plasma was aliquoted into tubes, frozen with liquid nitrogen, and stored at -80 °C. Plasma samples were then thawed on ice and EREG measured in duplicate using an enzyme-linked immunosorbant assay (ELISA) kit from Abcam (Cambridge, UK) according to manufacturer's instructions.

Immunohistochemistry

Naive mice were deeply anesthetized with sodium pentobarbital (60 mg/kg) and perfused transcardially through the left cardiac ventricle with 100 ml of perfusion buffer, followed by 250 ml of 4% paraformaldehyde (PFA) in 0.1 M phosphate buffer (PB), pH 7.4, at room temperature for 15 min. Subsequently, the spinal column was removed and post-fixed in the same fixative for 24 h at 4 °C. Spinal cord lumbar segments L3 and L4, and DRGs at the same levels were extracted and cryoprotected with 30% sucrose in 0.1 M PB. Tissue was embedded in an optimum cutting temperature medium (Tissue Tek OCT; Sakura), and 16-µm and 50-µm transverse DRG and spinal cord sections, respectively, were cut at -20 °C on a Leica CM3050 S cryostat. DRG sections were placed directly on gelatin-subbed slides and spinal cord sections were collected as free-floating sections in phosphate-buffered saline (PBS). The staining protocols for slides and free-floating tissue were similar. Sections were rinsed three times with PBS, with 0.2% Triton X-100 (PBS-T) for 10 min, and pre-incubated with 10% normal goat serum (NGS) for 1 h. To assess the colocalization between EGFR and markers of primary afferent neuronal populations, sections were incubated overnight at 4 °C in 5% NGS with either: 1) anti-EGFR raised in rabbit (1:50, Santa Cruz, #SC-03, Lot F1512) or 2) anti-EGFR and anti-NeuN raised in mouse (1:5000, Millipore, #MAB377, Lot 2062313). To assess the specificity of the EGFR antibody, the diluted antibody (1:50) was pre-incubated with the EGFR blocking peptide (1:5, Santa Cruz, #SC-03p, Lot E2109)

overnight at 4 °C in PBS before adding it to the tissue. The next day, tissue was washed three times with PBS-T for 10 min, incubated in Alexa 488 anti-rabbit (1:800, Invitrogen, #A11034, Lot 870976), Alexa 594 anti-guinea pig (1:800, Invitrogen, #A11076, Lot 714263), or Alexa 568 anti-mouse goat secondary antibodies (1:800, Invitrogen, #A11031, Lot 822389) in the dark for 2 h, and washed two times with PBS-T and one time with PBS. Free-floating sections were mounted on slides. All slides were coverslipped with Aqua-Poly/Mount (Polysciences). Sections were examined using a Zeiss LSM 510 confocal scanning laser microscope, equipped with Argon and Helium-Neon lasers using a multi-track approach.

Western blots

Tissue extracts for Western blotting were prepared in ice-cold homogenization buffer containing (in mM): 50 Tris-HCl, pH 7.4; 150 NaCl; 1 EDTA; 1% Triton X-100; 5 NaF; 1.5 Na_3VO_4 and protease inhibitor cocktail (complete, EDTA-free, Roche Applied Science, Indianapolis, IN). For measuring MMP-9, DRGs were removed from animals that were perfused transcardially with PBS. Following centrifugation at 12,000 × g for 10 min at 4 °C, the supernatant protein concentration was measured and equal protein quantities were boiled for 5 min in sample buffer and separated by SDS-PAGE. Following electrophoresis, proteins were transferred to 0.2 mm nitrocellulose membranes. Membranes were blocked in 5% dry milk powder in Tris-buffered saline containing 0.1% Tween-20 (TBS-T) for 1 h prior to overnight incubation with primary antibody. The membranes were then washed, incubated for 1 h with HRP-conjugated secondary antibody, washed again, treated with Enhanced Chemiluminescence reagent (Perkin Elmer) and exposed to autoradiography films (Denville Scientific Inc.). All signals were obtained in the linear range for each antibody, and densitometric analyses were performed with Image J (National Institutes of

Health, Bethesda, MD). Each phosphoprotein was normalized to the expression of the corresponding total protein. The antibodies and dilutions for the Western blots used in these studies are as follows: 4E-BP1 (1:1000, Cat. #9644, Cell Signaling Technology), p-4E-BP1 (Thr37/46) (1:1000, Cat. #2855, Cell Signaling Technology), AKT (1:1000, Cat. #4685, Cell Signaling Technology), p-AKT (Ser473) (1:1000, Cat#9271, Cell Signaling Technology), EGFR (1:1000, Cat. #sc-03, Santa Cruz Biotechnology), p-EGFR (1:1000, Cat. #3777, Cell Signaling Technology), MMP-9 (1:1000, Cat. #AB19016, Chemicon), S6 (1:1000, Cat. #sc-74459, Santa Cruz Biotechnology), p-S6 (Ser240/244) (1:1000, Cat. #2215, Cell Signaling Technology), and β-actin (1:5000, Cat. #A5441, Sigma).

Calcium imaging

Mouse lumbar DRG neurons (L3–L5; at least n=4 mice per condition) were harvested and cultured as previously described(46). Briefly, DRGs were isolated, transferred into Hank's Balanced Salt Solution (HBSS) and enzyme-digested by incubation with papain and collagenase type II (Worthington Biochemical Corp.). Dissociated neurons were plated on glass coverslips coated with poly-d-lysine and laminin and maintained at 37 °C at 5% CO_2/95% air in F12 media (Life Technologies) with 10% FBS. After 2–6 h, dissociated neurons on coverslips were loaded with 1 μM of the cell permeable calcium sensitive dye, Fura-2, AM (Life Technologies) for 30 min, and washed with HBSS before use. Coverslips were placed in a chamber containing HBSS at room temperature (20–22 °C) for recordings under following conditions: baseline (1-min recording, no solution); treated either with vehicle (DPBS) or EREG (200 ng/ml) for 10 min and then stimulated either with capsaicin (1 μM) or mustard oil (100 nM) for 30 s. Seventy-five mM KCl was added at the end of recordings, and only neurons with a positive KCl response were included in the

analysis. In the repeated capsaicin-pulse experiments, after baseline recording, 25 mM KCl was applied for 15 s followed by capsaicin (500 nM in HBSS) application for 15 s every 4 min as previously described (47). HBSS (vehicle) or EREG (200 ng/ml) was applied for 6 min after the fourth, fifth or sixth application of capsaicin, when the response had largely stabilized. After the incubation, three more pulses of capsaicin were applied and the ratio of the Ca^{2+} increases before and after exposure to EREG or HBSS was calculated as an index of enhancement. EREG caused sensitization in approximately 29% of capsaicin-responsive neurons (58 out of 197 capsaicin-stimulated cells). Fluorescence was detected by a Zeiss Observer Ratio Z1 microscope at 340 nm and 380 nm excitation wavelengths and analyzed with ZEN Black software (Zeiss). Cells were considered responsive to a drug infusion if the 340/380 ratio increase was ≥0.2 from baseline. Percentage of responsive neurons was determined for each coverslip and the average percentage values were compared statistically.

Quantitative real-time PCR

DRGs (L3–L4) were isolated and subjected to RNA extraction using TRIzol (Invitrogen, Burlington, ON). Reverse transcription was performed using a SuperScript III Reverse-Transcriptase Kit and Random Hexamers (Invitrogen) according to the manufacturer's instructions. qRT-PCRs were carried out in a CFX96-PCR system using iQ Sybr Green Supermix RT (Bio-Rad, Mississauga, ON) according to the manufacturer's instructions. The following primers were used: *Mmp9* (forward) GATCCCCAGAGCGTCATTC; *Mmp9* (reverse) CCACCTTGTTCACCTCATTTTG, *Gapdh* (forward) TCCATGACAACTTTGGCATTG; *Gapdh* (reverse) CAGTCTTCTGGGTGGCAGTGA. Analyses were carried out in triplicate and the *Mmp9* signal was normalized to *Gapdh*.

Polysomal profile analysis

Lumbar DRGs (L3–L5; pooled from at least *n*=10 mice per condition) were isolated and placed in ice-cold HEPES-KOH HBSS (Hank's Balanced Salt Solution, pH 7.4) containing 100 μg/ml cyclohexamide. HBSS was replaced with the ice-cold hypotonic lysis buffer(48) containing protease (complete EDTA-free, Roche Products) and RNase inhibitors (Rnasin, Promega, Madison, WI), and the tissue was subjected to brief homogenization using a glass homogenizer. The homogenated material was spun at 18,000 *g* for 2 min at 4 °C, and the supernatant loaded on a 10-50% w/w sucrose gradient in 20 mM HEPES-KOH, pH 7.6, 100 mM KCl and 5 mM $MgCl_2$, and centrifuged at 35,000 *g* for 2.5 h at 4 °C in an Optima L-80 XP ultracentrifuge (Beckman Coulter) using an SW40Ti rotor. Polysome analysis was performed by measuring the optical density (OD) at 254 nm using an ISCO fractionators (Teledyne ISCO; Lincoln, NE), as described previously (48). qRT-PCR analysis was performed as previously described (49). Sucrose gradient fractions were subjected to RNA extraction using TRIzol (Invitrogen). Reverse transcription was performed using a SuperScript III Reverse-Transcriptase Kit (Invitrogen) and Random Hexamers (Invitrogen) according to the manufacturer's instructions. qRT-PCRs were carried out in a CFX96 (Bio-Rad) RT-PCR system using iQ Sybr Green Supermix (Bio-Rad) according to the manufacturer's instructions using the following primers (*Mmp9* forward: GATCCCCAGAGCGTCATTC; *Mmp9* reverse: CCACCTTGTTCACCTCATTTTG). For all experiments *n*=4 (technical replicates); results are presented in arbitrary units as relative amounts using serial dilutions of DRG or spinal RNA as qRT-PCR concentration standards.

Drosophila experiments

Flies were reared on cornmeal-molasses-yeast agar at 25 °C, 70% humidity, on a 12:12-h light/dark cycle. *ppk-Gal4, Egfr* mutants $Egfr^{f24}$ and $Egfr^{tsla}$ lines were obtained from the Bloomington Drosophila Stock Centre (BDSC; Bloomington, IL). Wildtype w^{1118} and *Egfr* short hairpin RNA-interference (RNAi) (transformant ID 107130) flies were obtained from the VDRC (Vienna, Austria).

Larval nociceptive behavior was analysed according to previously described methods (24). Third instar larvae were transferred to a 100 mm petri dish containing a thin film of distilled water and allowed a 10-min rest period. After this time, they were touched on abdominal segments A4–A6 with a heat probe consisting of a sharpened soldering iron with the tip heated to 46 °C. The response time was recorded as the time elapsed between application of the heat probe and the elicitation of the characteristic nociceptive withdrawal response, a 360° rolling motion about the lateral axis. Both male and female flies (n=60/genotype) were tested on at least three different days.

Human subjects and phenotyping

Genotype and phenotype data from the OPPERA case-control study are available at the Database of Genotypes and Phenotypes (dbGaP), accession number: phs000762.v1.p1. The OPPERA cohort was recruited and phenotyped as detailed previously (50, 51), and described briefly here. Volunteers were recruited at four U.S. study sites. Cases (n=127) had examiner-verified TMD at enrollment; controls (n=731) were individuals who reported no significant history of TMD symptoms. Classification of TMD was based on the Research Diagnostic Criteria (RDC) for Temporomandibular Disorder (52). To increase genetic homogeneity of the cohorts, only

Caucasian subjects were analyzed in this study; results from the full cohort were extremely similar. An additional subgroup of "supercontrols" (*n*=231 Caucasians) was classified *post hoc* as TMD-free controls who experienced no tenderness during palpation of 8 masticatory muscles and two temporomandibular joints. Their genotypes were contrasted with 129 Caucasian TMD cases.

The TMD case-control cohort (26) included 200 TMD cases and 198 controls, using similar recruitment protocols and diagnostic criteria as OPPERA with the exception that enrollment was open to non-Hispanic Caucasian females age 18-45, and cases were recruited through a tertiary care pain clinic rather than from the general population.

The pre-OPPERA cohort (27) included *n*=186 initially pain-free Caucasian females age 18–34, of which 15 developed RDC-verified TMD over the course of the three year follow-up. Measures of sensitivity to multitude of pain-evoking stimuli have been also collected in all three cohorts (26, 27, 50, 51).

Only subjects who gave written, informed consent and provided a sample of blood for genotyping were included in the present analyses, and all study protocols were approved by the respective institutional review boards.

Genetic association

Genetic analysis of the OPPERA cohort was described previously (53). Genotyping was performed on DNA extracted from whole blood, using the Pain Research Panel (Algynomics Inc., Chapel Hill, NC). The Pain Research Panel is a microarray platform that assesses 3,295 SNP markers representing 358 genes of potential relevance to pain, inflammation, and/or mood and affect, as well as 160 ancestry informative markers used to adjust for population stratification. Duplicate study samples and HapMap reference DNA were genotyped to confirm accuracy and reliability of

genotyping, and quality filters were imposed for call rate >95%, reliability >99%, minor allele frequency >1%, and adherence to Hardy-Weinberg equilibrium. The overall call rate was 99.7%, with 2,924 SNPs passing quality filters. Genotyping of the pre-OPPERA cohort was performed separately on the Pain Research Panel using DNA from whole blood after amplification.

PLINK v.1.07 (Broad Institute, Cambridge, MA) software (54) was used to perform case-control association tests by logistic regression, assuming a co-dominant inheritance model. All tests on the OPPERA cohort controlled for recruitment site, and tests which included non-Caucasians also adjusted for race using the first two eigenvectors of a principal components analysis (PCA) on the genotype matrix (55).

After initial association tests performed in OPPERA identified *EREG* and *EGFR*, five SNPs from *EREG* and 25 SNPs from *EGFR* were extracted from the full SNP panel. Haplotype blocks were identified in each gene using Haploview v.4.2 (56), and tag SNPs were selected to cover haplotypic variation in *EREG* (rs2367707, rs7687621, rs1542466) and *EGFR* (5' region: rs759171, rs4947963; 3' region: rs1140475, rs2740762, rs845552). Haplotype testing was performed in the R statistical environment using logistic regression. Omnibus tests were used to detect differences in TMD odds between any major haplotype group, and *post hoc* tests were performed contrasting individual haplotypes against all others in order to characterize their effects. Combined *p*-values for haplotype analysis were calculated using the optimally weighted Z-test (57).

To explore cellular mechanisms underlying the associations, we applied bioinformatic pathway analysis (based on Pathway Studio, Elsevier) to identify signaling networks implicated by the association results in the discovery cohort. The multiple-testing-adjusted significance threshold was determined to be 0.002 for the 5% level, as determined through permutation (58).

Human mRNA studies

Leukocytes were obtained from 6 ml heparinized venous blood from human subjects. Briefly, whole blood was diluted in endotoxin-free RPMI-1640 medium and centrifuged through Ficoll/Histopaque 1077 (Sigma Chemical Co., St Louis, MO), and the buffy coat cells were washed five times with sterile isotonic saline. Total RNA was isolated with Trisol Reagent (Life Technologies, Grand Island, NY) and RT-PCR was performed analyzed with the SABioscience Custom PCR array system (Valencia, CA). The cDNAs from all participants were normalized to GAPDH through dilution to the concentration at which GAPDH gave an equal signal in RT-PCR reactions.

Human cDNA amplified from study participants with the major *EREG* haplotype was cloned into pCDNA3 vectors under a CMV-promoter to generate a wildtype expression *EREG* plasmid (gift from Dr. Oskar Laur, Emory University, Atlanta GA). Briefly, an expression plasmid with the minor allele at rs2367707 was generated by site-directed mutagenesis. Expression plasmids were transiently transfected into HEK293 cells using Lipofectamine 2000 (Life Technologies) in accordance with manufacture's recommendations. The time course of mRNA degradation was measured after actinomycin D (actD; Sigma) treatment. Thirty-six hours after transfection of *EREG* plasmids, cells were treated with actD (10 μg/ml) and collected at 0, 2, 4, or 6 h post treatment. Total RNA was isolated after each time point using Trizol reagent (Life Technologies). The isolated RNA was treated with RNase free-DNase I (Promega) and reverse transcribed using a SuperScript III Reverse-Transcriptase Kit (Invitrogen) and Random Hexamers (Invitrogen) according to the manufacturer's instructions. qRT-PCRs were carried out in a CFX96 (Bio-Rad) RT-PCR system using iQ Sybr Green Supermix (Bio-Rad) according to the manufacturer's instructions. cDNAs of *EREG* and the housekeeping gene, *GAPDH*, were amplified using forward

and reverse PCR primers (GGCTATTGTTTGCATGGACAG and CACGGTCAAAGCCACATATTC, for *EREG*; and CTTTGGTATCGTGGAAGGACTC and GTAGAGGCAGGGATGATGTTC, for *GAPDH*). Two independent experiments were conducted in triplicate. Data were normalized to *GAPDH*.

Statistical analyses

Data were analyzed by two-tailed Student's *t*-test (unless otherwise indicated), one-way or two-way ANOVA (or Kruskal-Wallis ANOVA by ranks), followed where appropriate by Tukey's HSD posthoc test or Dunnett's case-comparison posthoc test. A *P* value less than 0.05 was considered significant. Four data points were excluded based on their identification as statistical outliers (Studentized residuals >3). AD_{50}s and associated 95% confidence intervals were calculated using the FlashCalc 40.1® macro (M.H. Ossipov, University of Arizona). As we had no *a priori* expectation of effect sizes, power analyses were not used to calculate sample sizes. Instead, we adhered to standard practices in the field (59). In many cases, sample sizes were dictated by breeding success.

Study approval

Mice were maintained in the animal facilities of McGill University and the University of Toronto Mississauga. All mouse experiments were approved and performed in accordance with relevant local animal care and use committees according to the Canadian Council on Animal Care (CCAC) guidelines. The OPPERA study was reviewed and approved by Institutional Review Boards at each of the 4 study sites and at the data coordinating center: University at Buffalo (Buffalo, NY); University of Maryland (Baltimore, MD); University of North Carolina at Chapel Hill (Chapel

Hill, NC); University of Florida (Gainesville, FL); and the Battelle Memorial Institute (Durham, NC). All participants verbally agreed to a screening interview done by telephone and they provided informed, signed consent for all other study procedures.

AUTHOR CONTRIBUTIONS

J.S.M., and L.D. conceived of the initial project with input from L.J.M., and S.B.S. L.J.M., and J.S.M. designed the majority of the animal experiments. L.J.M., S.B.S., A.K., C.A.M., A.S., R.E.S., C.C., N.Y., S.S., S.T., T.C., T.H.K., E.M., D.G.G., J.S.W., S.G.S., and J-S.A. performed research. S.B.S. and L.D. performed the bioinformatics analysis on the OPPERA data set. L.J.M., S.B.S., A.K., C.A.M., V.O., C.B.M., A.S., J.H.G., A.G.N., A.R., G.G.N., D.V.Z., J.S.M., and L.D., analyzed the data. J.G., R.B.F., R.O., G.D.S., C.K., R.D., W.M., and L.D. provided clinical data. C.G., N.S., L.G., A.G.N., A.R., and G.G.N., oversaw portions of this project. L.J.M., S.B.S., J.S.M., and L.D. wrote the paper with input from all authors.

ACKNOWLEDGMENTS

The authors would like thank Dr. Oskar Laur for creating *EREG*-expressing constructs at the Custom Cloning Core Facility, Emory University. This research was supported by the Canadian Institutes for Health Research (N.S., M.W.S., L.G., A.R., Y.D.K. and J.S.M.), the U.S. National Institutes of Health (J.G., R.B.F., R.O., G.D.S., C.K., R.D., W.M., D.Z., and L.D.), the Australian NHMRC (T.C., T.M.K., G.G.N.), and the Louise and Alan Edwards Foundation (J.S.M.). Loren Martin was supported by postdoctoral fellowships from CIHR and the Canadian Pain Society.

CONFLICT OF INTEREST STATEMENT

Shad B. Smith, Roger B. Fillingim, Gary D. Slade and Jeffrey S. Mogil are consultants and equity stock holders, and William Maixner and Luda Diatchenko are cofounders and equity stock holders in Algynomics, Inc., a company providing research services in personalized pain medication and diagnostics.

SUPPLEMENTAL INFORMATION

Supplemental Information includes 8 Figures and 5 Tables and a methods section and are available in the online version of this paper.

REFERENCES

1. Elliot, AM, Smith, BH, Penny, KI, Smith, WC, and Chambers, WA. The epidemiology of chronic pain in the community. *Lancet*. 1999;354:1248-1252.

2. Gereau, RWI, Sluka, KA, Maixner, W, Savage, SR, Price, TJ, et al. A pain research agenda for the 21st century. *J Pain*. 2014;15:1203-1214.

3. Medicine, Io. 2011. *Relieving Pain in America: A Blueprint for Transforming Prevention, Care, Education, and Research*. Washington, D.C.: National Academies Press.

4. Erschbamer, M, Pernold, K, and Olson, L. Inhibiting epidermal growth factor receptor improves structural, locomotor, sensory, and bladder recovery from experimental spinal cord injury. *J Neurosci*. 2007;27:6428-6435.

5. Kersten, C, Cameron, MG, and Mjaland, S. Epithelial growth factor receptor (EGFR)-inhibition for relief of neuropathic pain--A case series. *Scand J Pain*. 2013;4:3-7.

6. Kersten, C, and Cameron, MG. Cetuximab alleviates neuropathic pain despite tumour progression. *BMJ Case Rep*. 2012;pii: bcr1220115374.

7. Moryl, N, Obbens, EA, Ozigbo, OH, and Kris, MG. Analgesic effect of gefitinib in the treatment of non-small cell lung cancer. *J Support Oncol*. 2006;4:111.

8. Kersten, C, Cameron, MG, Laird, B, and Mjaland, S. Epidermal growth factor receptor-inhibition (EGFR-I) in the treatment of neuropathic pain. *Br J Anaesth*. 2015;115:761-767.

9. Citri, A, and Yarden, Y. EGF-ERBB signalling: towards the systems level. *Nat Rev Mol Cell Biol*. 2006;7:505-516.

10. Pastore, S, Mascia, F, Mariani, V, and Girolomoni, G. The epidermal growth factor receptor system in skin repair and inflammation. *J Invest Dermatol*. 2008;128:1365-1374.

11. Shirakata, Y, Komurasaki, T, Toyoda, H, Hanakawa, Y, Yamasaki, K, et al. Epiregulin, a novel member of the epidermal growth factor family, is an autocrine growth factor in normal human keratinocytes. *J Biol Chem*. 2000;275:5748-5753.

12. Kaganoi, J, Watanabe, G, Okabe, M, Nagatani, S, Kawabe, A, et al. STAT1 activation-induced apoptosis of esophageal squamous cell carcinoma cells in vivo. *Ann Surg Oncol*. 2007;14:1405-1415.

13. Zhang, Y, Zheng, L, Zhang, J, Dai, B, Wang, N, et al. Antitumor activity of taspine by modulating the EGFR signaling pathway of Erk1/2 and Akt in vitro and in vivo. *Planta Med*. 2011;77:1774-1781.

14. Wells, A, Gupta, K, Chang, P, Swindle, S, Glading, A, et al. Epidermal growth factor receptor-mediated motility in fibroblasts. *Microsc Res Tech*. 1998;43:395-411.

15. Chen, Y, Long, H, Wu, Z, Jiang, X, and Ma, L. EGF transregulates opioid receptors through EGFR-mediated GRK2 phosphorylation and activation. *Mol Biol Cell*. 2008;19:2973-2983.

16. Liu, X, Wu, WK, Yu, L, Li, ZJ, Sung, JJ, et al. Epidermal growth factor-induced esophageal cancer cell proliferation requires transactivation of beta-adrenoceptors. *J Pharmacol Exp Ther*. 2008;326:69-75.

17. Yang, H, Wang, Z, Capo-Aponte, JE, Zhang, F, Pan, Z, et al. Epidermal growth factor receptor transactivation by the cannabinoid receptor (CB1) and transient receptor potential vanilloid 1 (TRPV1) induces differential responses in corneal epithelial cells. *Exp Eye Res*. 2010;91:462-471.

18. Kawasaki, Y, Xu, Z-Z, Wang, X, Park, JY, Zhuang, Z-Y, et al. Distinct roles of matrix metalloproteases in the early- and late-phase development of neuropathic pain. *Nat Med*. 2008;14:331-336.

19. Pareja, M, Sanchez, O, Lorita, J, Soley, M, and Ramirez, I. Activated epidermal growth factor receptor (ErbB1) protects the heart against stress-induced injury in mice. *Am J Physiol Regul Integr Comp Physiol*. 2003;285:R455-R462.

20. Keith, RL, Karoor, V, Mozer, AB, Hudish, TM, Le, M, et al. Chemoprevention of murine lung cancer by gefitinib in combination with prostacyclin synthase overexpression. *Lung Cancer*. 2010;70:37-42.

21. Konecny, GE, Pegram, MD, Venkatesan, N, Finn, R, Yang, G, et al. Activity of the dual kinase inhibitor lapatinib (GW572016) against HER-2-overexpressing and trastuzumab-treated breast cancer cells. *Cancer Res*. 2006;66:1630-1639.

22. Lee, TC, and Threadgill, DW. Generation and validation of mice carrying a conditional allele of the epidermal growth factor receptor. *Genesis*. 2009;47:85-92.

23. Livneh, E, Glazer, L, Segal, D, Schlessinger, J, and Shilo, BZ. The *Drosophila* EGF receptor gene homolog: conservation of both hormone binding and kinase domains. *Cell*. 1985;40:599-607.

24. Tracey, WD, Jr., Wilson, RI, Laurent, G, and Benzer, S. *painless*, a *Drosophila* gene essential for nociception. *Cell*. 2003;113:261-273.

25. Maixner, W, Diatchenko, L, Dubner, R, Fillingim, RB, Greenspan, JD, et al. Orofacial pain prospective evaluation and risk assessment study--the OPPERA study. *J Pain*. 2011;12 (11 Wuppl.):T4-11.e11-12.

26. Slade, GD, Conrad, MS, Diatchenko, L, Rashid, NU, Zhong, S, et al. Cytokine biomarkers and chronic pain: association of genes, transcription, and circulating proteins with temporomandibular disorders and widespread palpation tenderness. *Pain*. 2011;152:2802-2812.

27. Diatchenko, L, Nackley, AG, Tchivileva, IE, Shabalina, SA, and Maixner, W. Genetic architecture of human pain perception. *Trends Genet*. 2007;23:605-613.

28. Cao, C, Huang, X, Han, Y, Wan, Y, Birnbaumer, L, et al. Galpha(i1) and Galpha(i3) are required for epidermal growth factor-mediated activation of the Akt-mTORC1 pathway. *Sci Signal*. 2009;2:ra17.

29. Obara, I, Tochiki, KK, Geranton, SM, Carr, FB, Lumb, BM, et al. Systemic inhibition of the mammalian target of rapamycin (mTOR) pathway reduces neuropathic pain in mice. *Pain*. 2011;152:2582-2595.

30. Xu, Q, Fitzsimmons, B, Steinauer, J, O'Neill, A, Newton, AC, et al. Spinal phosphinositide 3-kinase-Akt-mammalian target of rapamycin signaling cascades in inflammation-induced hyperalgesia. *J Neurosci*. 2011;31:2113-2124.

31. Obata, K, Yamanaka, H, Kobayashi, K, Dai, Y, Mizushima, T, et al. Role of mitogen-activated protein kinase activation in injured and intact primary afferent neurons for mechanical and heat hypersensitivity after spinal nerve ligation. *J Neurosci*. 2004;24:10211-10222.

32. Murooka, TT, Rahbar, R, Platanias, LC, and Fish, EN. CCL5-mediated T-cell chemotaxis involves the initiation of mRNA translation through mTOR/4E-BP1. *Blood*. 2008;111:4892-4901.

33. Andres, C, Meyer, S, Dina, OA, Levine, JD, and Hucho, T. Quantitative automated microscopy (QuAM) elucidates growth factor specific signalling in pain sensitization. *Mol Pain*. 2010;6:98.

34. Heldin, CH. Dimerization of cell surface receptors in signal transduction. *Cell*. 1995;80:213-223.

35. Weiss, A, and Schlessinger, J. Switching signals on or off by receptor dimerization. *Cell*. 1998;94:277-280.

36. Riese, DJ, 2nd, Komurasaki, T, Plowman, GD, and Stern, DF. Activation of ErbB4 by the bifunctional epidermal growth factor family hormone epiregulin is regulated by ErbB2. *J Biol Chem*. 1998;273:11288-11294.

37. Shelly, M, Pinkas-Kramarski, R, Guarino, BC, Waterman, H, Wang, LM, et al. Epiregulin is a potent pan-ErbB ligand that preferentially activates heterodimeric receptor complexes. *J Biol Chem*. 1998;273:10496-10505.

38. Kurtze, I, Sonnemann, J, and Beck, JF. KRAS-mutated non-small cell lung cancer cells are responsive to either co-treatment with erlotinib or gefitinib and histone deacetylase inhibitors or single treatment with lapatinib. *Oncol Rep*. 2011;25:1021-1029.

39. Lu, PH, Kuo, TC, Chang, KC, Chang, CH, and Chu, CY. Gefitinib-induced epidermal growth factor receptor (EGFR)-independent keratinocyte apoptosis is mediated by the JNK-activation pathway. *Br J Dermatol*. 2010;164:38-46.

40. Dunham, NW, and Miya, TS. A note on a simple apparatus for detecting neurological deficit in rats and mice. *J Am Pharm Assoc*. 1957;46:208-209.

41. Hargreaves, K, Dubner, R, Brown, F, Flores, C, and Joris, J. A new and sensitive method for measuring thermal nociception in cutaneous hyperalgesia. *Pain*. 1988;32:77-88.

42. Chaplan, SR, Bach, FW, Pogrel, JW, Chung, JM, and Yaksh, TL. Quantitative assessment of tactile allodynia evoked by unilateral ligation of the fifth and sixth lumbar nerves in the rat. *J Neurosci Meth*. 1994;53:55-63.

43. Decosterd, I, and Woolf, CJ. Spared nerve injury: an animal model of persistent peripheral neuropathic pain. *Pain*. 2000;87:149-158.

44. Bennett, GJ, and Xie, Y-K. A peripheral mononeuropathy in rat that produces disorders of pain sensation like those seen in man. *Pain*. 1988;33:87-107.

45. Hylden, JLK, and Wilcox, GL. Intrathecal morphine in mice: a new technique. *Eur J Pharmacol*. 1980;67:313-316.

46. Malin, SA, Davis, BM, and Molliver, DC. Production of dissociated sensory neuron cultures and considerations for their use in studying neuronal function and plasticity. *Nat Protoc*. 2007;2:152-160.

47. Bonnington, JK, and McNaughton, PA. Signalling pathways involved in the sensitisation of mouse nociceptive neurones by nerve growth factor. *J Physiol*. 2003;551:433-446.

48. Mamane, Y, Petroulakis, E, Martineau, Y, Sato, TA, Larsson, O, et al. Epigenetic activation of a subset of mRNAs by eIF4E explains its effects on cell proliferation. *PLoS One*. 2007;2:e242.

49. Parsyan, A, Shahbazian, D, Martineau, Y, Petroulakis, E, Alain, T, et al. The helicase protein DHX29 promotes translation initiation, cell proliferation, and tumorigenesis. *Proc Natl Acad Sci U S A*. 2009;106:22217-22222.

50. Slade, GD, Bair, E, By, K, Mulkey, F, Baraian, C, et al. Study methods, recruitment, sociodemographic findings, and demographic representativeness in the OPPERA Study. *J Pain*. 2011;12:T12-26.

51. Ohrbach, R, Fillingim, RB, Mulkey, F, Gonzalez, Y, Gordon, S, et al. Clinical findings and pain symptoms as potential risk factors for chronic TMD: descriptive data and empirically identified domains from the OPPERA case-control study. *J Pain*. 2011;12 (11 Suppl.):T27-T45.

52. Dworkin, S, and LeResche, L. Research diagnostic criteria for temporomandibular disorders: review, criteria, examinations and specifications, critique. *J Craniomandib Disord*. 1992;6:301-355.

53. Smith, SB, Maixner, DW, Greenspan, JD, Dubner, R, Fillingim, RB, et al. Potential genetic risk factors for chronic TMD: genetic associations from the OPPERA case control study. *J Pain*. 2011;12:T92-T101.

54. Purcell, S, Neale, B, Todd-Brown, K, Thomas, L, Ferreira, MAR, et al. PLINK: a toolset for whole-genome association and population-based linkage analysis. *Am J Hum Genet*. 2007;81:559-575.

55. Price, AL, Patterson, NJ, Plenge, RM, Weinblatt, ME, Shadick, NA, et al. Principal components analysis corrects for stratification in genome-wide association studies. *Nat Genet*. 2006;38:904-909.

56. Barrett, JC, Fry, B, Maller, J, and Daly, MJ. Haploview: analysis and visualization of LD and haplotype maps. *Bioinformatics*. 2005;21:263-265.

57. Zaykin, DV. Optimally weighted Z-test is a powerful method for combining probabilities in meta-analysis. *J Evol Biol*. 2011;24:1836-1841.

58. Slade, GD, Smith, SB, Zaykin, DV, Tchivileva, IE, Gibson, DG, et al. Facial pain with localized and widespread manifestations: separate pathways of vulnerability. *Pain*. 2013;154:2335-2343.

59. Mogil, JS, Ritchie, J, Sotocinal, SG, Smith, SB, Croteau, S, et al. Screening for pain phenotypes: analysis of three congenic mouse strains on a battery of nine nociceptive assays. *Pain*. 2006;126 24-34.

FIGURE LEGENDS

Figure 1. EGFR antagonists produce analgesia and EREG produces hyperalgesia in the mouse. (**A**) No sedation or ataxia (two-way ANOVA, drug x repeated measures: $F_{12,80}$=0.5, p=0.88) produced by high doses of EGFR antagonists. Symbols represent mean ± SEM latency (s) to fall off rotarod at each time point; n=6–8/drug. (**B**) No effect of EGFR antagonists on acute thermal pain measured using the radiant heat paw-withdrawal test (two-way ANOVA, drug x repeated measures: $F_{3,19}$=2.3, p=0.10). Bars represent mean ± SEM latency (s) to withdraw from a noxious thermal stimulus before (baseline) and 30 min after (post-drug) injection; n=5–6/drug. (**C**) No effect of EGFR antagonists on acute mechanical sensation using the von Frey test (two-way ANOVA, drug x repeated measures: $F_{3,19}$=0.3, p=0.80). Bars represent mean ± SEM hind paw withdrawal threshold (g) before (baseline) and 30 min after (post-drug) injection; n=5–6/drug. (**D**) EGFR antagonists produce analgesia on the formalin test in both the early (0–10 min; one-way ANOVA, $F_{3,29}$=7.2, p=0.001) and late (10–60 min; one-way ANOVA, $F_{3,29}$=15.9, p<0.001) phases. Bars represent mean ± SEM percentage of samples featuring licking/biting behavior; n=7–9/drug. (**E**) Dose-dependent analgesia from EGFR antagonists and morphine on the late-phase formalin test; symbols represent mean ± SEM percentage of samples featuring licking/biting behavior; n=6–8/drug/dose. See Supplemental Table 1 for half-maximal analgesic doses and 95% confidence intervals. (**F**) EGFR antagonists reverse thermal hypersensitivity induced by carrageenan (two-way ANOVA, drug x repeated measures: $F_{9,57}$=2.8, p=0.01). Symbols represent mean ± SEM latency (s) to withdraw from a noxious thermal stimulus before carrageenan (Pre-BL), 3 h after carrageenan (0), and 20–60 min post-drug; n=5–6/drug. (**G**) EGFR antagonists dose-dependently reverse mechanical allodynia induced by complete Freund's adjuvant (CFA; 3 days post-injection). Symbols represent mean ± SEM percentage of maximum possible

anti-allodynia (i.e., reversal back to baseline withdrawal thresholds at all post-drug time points; see Methods); n=5–6/drug/dose. (**H**) EGFR antagonists dose-dependently reverse mechanical allodynia induced by spared nerve injury (SNI; 7 days post-surgery). Symbols as in **G**; n=5–6/drug/dose. See Supplemental Table 2 for half-maximal analgesic doses and 95% confidence intervals relevant to graphs **G, H**. (**I**) AG 1478 reverses mechanical allodynia induced by chronic constriction injury (CCI; 14 days post-surgery); n=6/drug (two-way ANOVA, drug x repeated measures: $F_{4,40}$=2.6, p=0.02). For all panels, *p<0.05, **p<0.01, ***p<0.001 compared to vehicle (0) group by Dunnett's case-comparison posthoc test.

Figure 2. Spinally administered EREG, but not other EGFR ligands, produces hypersensitivity. (**A**) Significant and dose-dependent hypersensitivity from EREG (two-way ANOVA, $F_{3,26}$=6.8, p=0.002), but not betacellulin, amphiregulin, EGF or TGF-α (all p's>0.50) in the late phase (10–60 min) of the formalin test. Symbols represent mean ± SEM percentage of samples featuring licking/biting behavior; n=6–8/drug/dose. EREG enhancement of formalin-induced licking was equivalent to that of nerve growth factor (NGF); two-way ANOVA, $F_{3,22}$=10.9, p<0.001. (**B**) EREG (10 ng, i.t.) increases nocifensive behavior when co-administered with intraplantar injections of the TRPV1 agonist capsaicin (two-tailed *t-test*, t_{10}=3.4, p=0.01) but not the TRPA1 agonist mustard oil (two-tailed *t-test*, t_{13}=0.34, p=0.70). Bars represent mean ± SEM duration of licking behavior (s) over 10 min post-injection; n=6-8/algogen/drug. (**C**) The TRPV1 antagonist, AMG 9810 (30 mg/kg, i.p.), but not the TRPA1 antagonist, HC-030031 (30 mg/kg, i.p.) blocks EREG-induced hyperalgesia on the formalin test (two-way ANOVA, drug x antagonist interaction: $F_{2,38}$=7.2, p=0.002). Bars as in graph **A**; n=7-8/group. (**D**) EREG (10 ng) increases thermal sensitivity by itself (two-tailed paired *t-test*, t_{10}=2.6, p=0.03). Bars represent

mean ± SEM latency (s) to withdraw from a noxious thermal stimulus before (baseline) and 30 min after (post-drug) injection; *n*=6/drug. (**E**) EREG (10 ng) increases mechanical sensitivity by itself (two-tailed paired *t-test*, t_{10}=2.2, *p*=0.05). Bars represent mean ± SEM hind paw withdrawal threshold (g) before (baseline) and 30 min after (post-drug) injection; *n*=6/drug. (**F**) ΔEGFR mutants have higher baseline pain sensitivity to formalin than wildtypes (vehicle groups), but no longer respond to EREG (10 ng, i.t.). Bars as in graph **E**; *n*=7–8/genotype/drug. For all panels, **p*<0.05, ***p*<0.01, ****p*<0.001 compared to vehicle (0) by Dunnett's case-comparison posthoc test or *t*-test as indicted. •• *p*<0.01 compared to other genotype (in **F**) by Dunnett's case-comparison posthoc test.

Figure 3. Genetic association of *EREG* and *EGFR* with TMD pain. Genetic association of *EREG* (**A**) and *EGFR* (**B**) SNPs with chronic TMD pain in OPPERA Cases vs. Supercontrols ("SC"), OPPERA Cases vs. Controls ("all"), TMD Case-Control cohort, and pre-OPPERA cohorts (see Materials and Methods). Manhattan plots and corresponding gene loci are shown where position of tested SNPs is given relative to gene structure. Non-synonymous (red), synonymous (green), promoter region (grey) and 3' intragenic region (blue) SNPs are indicated. The pattern of association within the *EREG* gene locus was identical in all cohorts. The pattern of association for *EGFR* gene locus revealed some differences between cohorts; however, the 5' and 3' ends of the gene consistently showed association with elevated TMD risk. The *EGFR* SNPs showing association in independent SNP tests (marked in bold) were used for haplotype analysis (see Supplementary Table 5). (**C**) Forest plot depicting odds ratios (OR; with 95% confidence intervals) for minor allele T of rs1563826 in four human chronic pain cohorts. (**D**) Association of *EREG* mRNA level with *EREG* rs1563826 in the TMD case-control cohort measured by quantitative

RT-PCR. Bars represent mean ± SEM *EREG* expression in leukocytes expressed in arbitrary units relative to *GAPDH* (see Materials and Methods). One-way ANOVA revealed a significant difference among genotypes; $F_{2,247}$=3.7, p=0.03. *p<0.05; the A/A versus T/T comparison was p=0.053, likely due to the small number of T/T homozygotes. **(E)** Following actinomycin D (actD) treatment, the rate of mRNA degradation was significantly lower for cells expressing wildtype (WT; G allele) *EREG* mRNA compared to those the minor A allele of rs2367707 (two-tailed paired *t-test*, t_4=2.8, p=0.05). Symbols represent mean ± SEM percentage mRNA expression compared to time 0; n=3/genotype.

Figure 4. EREG and EGFR are upregulated in chronic pain states, and EREG increases activation of medium-small DRG sensory neurons. (**A**) EREG in the blood is upregulated by CFA and SNI, but not formalin ($F_{3,38}$=10.0, p<0.001) as measured by ELISA. Bars represent mean ± SEM protein levels (pg/ml); n=9–10 biological replicates/group. One-way ANOVA followed by Dunnett's case-comparison post-hoc test, *p<0.05, ***p<0.001 compared to control group. (**B**) EGFR (green) is abundantly found in all DRG sensory neurons. Scale bar = 50 μm. (**C**) The cellular distribution of EGFR is equal among different cell sizes that exhibit either high or low EGFR staining. (**D**) **Top:** Representative Western blots showing phosphorylated (p-)EGFR and β-actin in the DRG before (BL) (left band) and 3 days (3d) or 7 days (7d) after CFA or SNI, respectively (right band). **Bottom:** Quantification of Western blot data (n=5 biological replicates/condition), after normalization to β-actin and compared to baseline values. *p<0.05 compared to 1.0 by one-tailed t-test (CFA: t_4=2.5, p=0.03; SNI: t_4=3.3, p=0.02. (**E**) Fluorescence microscopic images (Fura-2 340/380-nm ratio) of DRG neurons from naïve mice at baseline (top row, 1-min recording); treated either with vehicle (Veh; DPBS) or EREG (200 ng/ml) for 10 min (second row)

and then stimulated either with the TRPV1 agonist, capsaicin (Cap, 1 μM) or the TRPA1 agonist, mustard oil (MO, 100 nM) for 30 s (third row). KCl (75 mM) was added at the end of recordings and only neurons with a positive KCl response were included in the analysis. Scale bars = 50 μm. (**F**) The 340/380-nm ratio increase from the baseline before application of Cap or MO to the peak maximum after application (Δ ratio). Bars represent mean ± SD of delta ratio of responsive neurons treated either with Vehicle+Cap, EREG+Cap, Veh+MO, or EREG+MO; *n*=34-36/group. Two-way ANOVA, algogen x vehicle/EREG: $F_{3,136}$ = 16.2, p<0.001). Unpaired Student's *t*-test, ***p<0.001. (**G**) Representative calcium traces of neurons responsive to multiple capsaicin (500 nM, 15 sec for every 4 min) pulses and treated either with vehicle (HBSS, left figure) or EREG (200 ng/ml, right figure) for 6 min before three challenging pulses of capsaicin were applied. The ratio of Ca^{2+} peak heights (b/a) before and after exposure to EREG or vehicle was calculated as a measure of signal enhancement. (**H**) EREG but not vehicle enhanced the TRPV1 currents of capsaicin challenge pulses. Data presented as mean ± SEM, *n*=45-58/group, from a total of 9/13 experiments for vehicle/EREG. Unpaired Student's *t*-test, ***p<0.001.

Figure 5. EREG/EGFR increases pain through a PI3K/AKT→mTOR→4E-BP1→eIF4F complex→MMP-9 signaling pathway. (**A**) The signaling pathway investigated, with major proteins indicated in black and blocking drugs or mutants shown in red. (**B**) Treatment with wortmannin (5 μg, i.t.) blocks EREG-induced increases in late-phase formalin-induced pain behavior (drug x drug: $F_{1,23}$ = 4.7, p=0.04). (**C**) Low doses of rapamycin (5 mg/kg) and CCI 779 (1 mg/kg) block EREG effects without affecting formalin-induced pain *per se* (rapamycin, drug x drug: $F_{1,27}$ = 3.6, p=0.04; CCI 779 drug x drug: $F_{1,28}$ = 4.2, p=0.03); higher doses (10 mg/kg) are analgesic (main effects: rapamycin, $F_{1,28}$ = 22.9, p<0.001; CCI 779, $F_{1,28}$ = 30.2, p<0.001). (**D**) No effect on EREG increases in formalin-induced pain behavior in SGK1/2 (*Rps6kb1/Rps6kb2*)

double null mutant mice (*Rps6kb1/2*$^{-/-}$; main effect of drug: $F_{1,18}$ = 25.8, p<0.001). (**E**) Lack of EREG effects in 4E-BP1 (*Eif4ebp1*$^{-/-}$) null mutant mice (genotype x drug: $F_{1,33}$ = 7.1, p=0.01). (**F**) Treatment with 4EGI-1 (25 μg, i.t.) blocks EREG effects (drug x drug: $F_{1,20}$ = 7.6, p=0.01). (**G**) Treatment with TIMP-1 (4 pmol, i.t.) blocks EREG effects (drug x drug: $F_{1,30}$ = 5.6, p=0.02). (**H**) Lack of EREG effects in MMP-9 null mutants (*Mmp9*$^{-/-}$; genotype x drug: $F_{1,20}$ = 16.1, p=0.001). In all experiments, EREG was injected at 10 ng, i.t. Bars in all graphs represent mean ± SEM percentage of samples featuring licking/biting behavior; n=6–8/drug/dose and n=6–12/drug/genotype (dependent on breeding success). Two-way ANOVA for all panels followed by *t-test* compared to EREG vehicle, *p<0.05, **p<0.01, ***p<0.001; compared to wortmannin, rapamycin, CCI 779, 4EGI-1 or TIMP-1 vehicle, or +/+ genotype •p<0.05, ••p<0.01, •••p<0.001; compared to rapamycin/CCI 779 vehicle °p<0.05.

Figure 6. EREG and formalin induce phosphorylation of AKT and 4EBP-1 and increase the expression of MMP-9 in lumbar DRG tissue. EREG (10 ng, i.t.) or 5% formalin (20 μl, intraplantar) was injected and lumbar DRG tissue harvested 40 min later. Rapamycin was injected 20 min before EREG or formalin to mimic behavioral experiment parameters. (**A**) Representative Western blots showing the phosphorylated (p-) and total protein abundance for AKT, 4E-BP1 and S6. The total amount of MMP-9 is also presented. Quantification (phosphorylated/total) for the percent-fold increase (compared to the control condition) in phosphorylated AKT, 4E-BP1, and S6 is presented in panels **B**–**D** along with the quantification for total MMP-9 (panel **E**), bars represent mean ± SEM for relative change in protein expression. (**B**) EREG significantly increases the phosphorylation of AKT in DRG tissue. (**C**) Both formalin and EREG increase the phosphorylation of 4E-BP-1, and the increases are blocked by rapamycin. (**D**) The phosphorylation

of S6 is significantly elevated relative to control tissue by EREG treatment, an increase blocked by rapamycin. (**E**) Formalin and EREG significantly increase MMP-9 expression and these increases are blocked by rapamycin. Sample sizes in all groups are n=4–6. One-way ANOVA for all panels followed by Dunnett's case-comparison post-hoc test, *p<0.05, **p<0.01, ***p<0.001 compared to control tissue. †p<0.05 decrease compared to EREG or formalin alone group. •p<0.05 increase compared to EREG or formalin alone group.

SUPPLEMENTARY MATERIALS

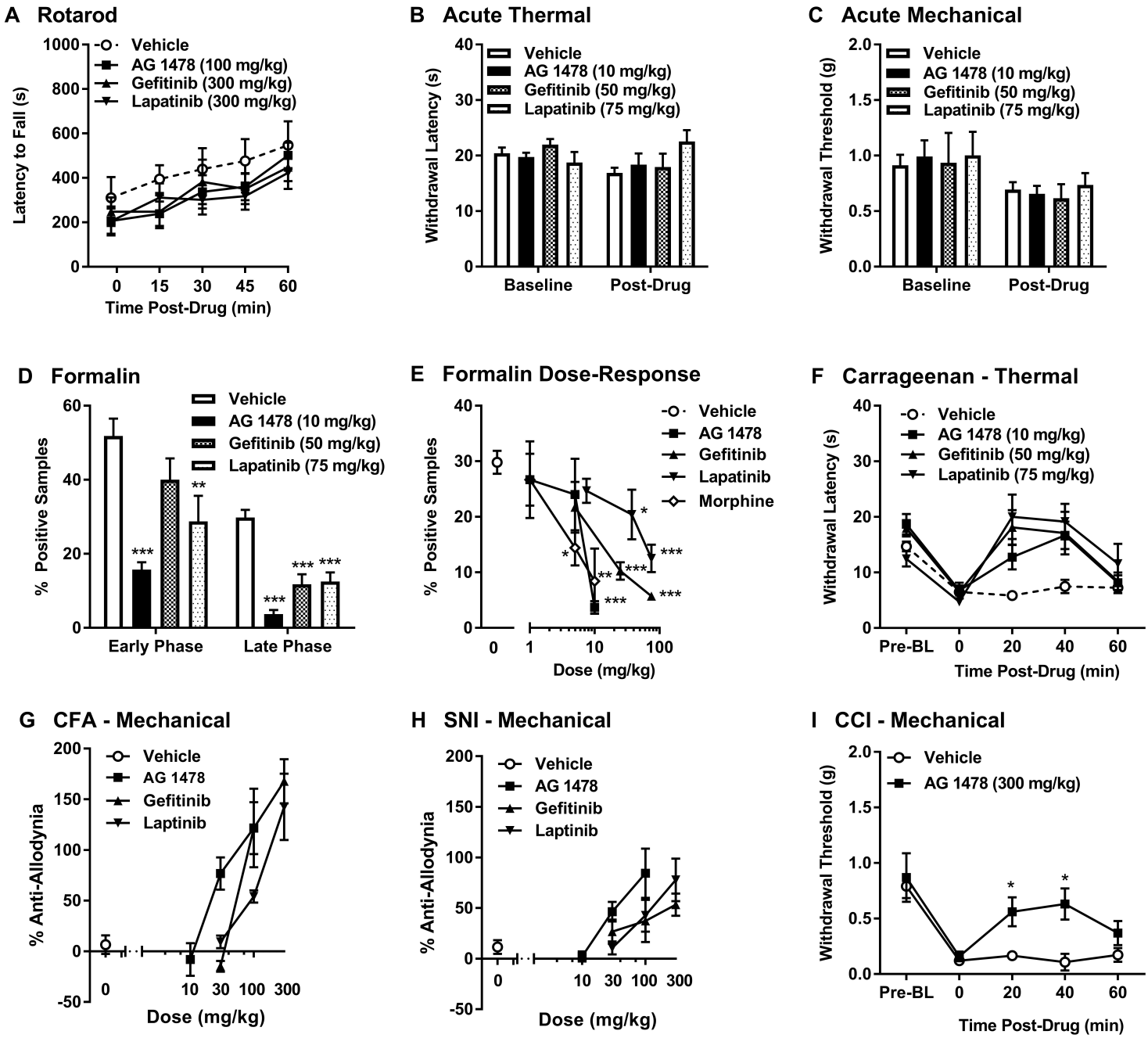
A Rotarod
Vehicle
AG 1478 (100 mg/kg)
Gefitinib (300 mg/kg)
Lapatinib (300 mg/kg)
Latency to Fall (s)
Time Post-Drug (min)
B Acute Thermal
Vehicle
AG 1478 (10 mg/kg)
Gefitinib (50 mg/kg)
Lapatinib (75 mg/kg)
Withdrawal Latency (s)
Baseline
Post-Drug
C Acute Mechanical
Withdrawal Threshold (g)
D Formalin
% Positive Samples
Early Phase
Late Phase
E Formalin Dose-Response
Vehicle
AG 1478
Gefitinib
Lapatinib
Morphine
Dose (mg/kg)
F Carrageenan - Thermal
Pre-BL
G CFA - Mechanical
% Anti-Allodynia
H SNI - Mechanical
I CCI - Mechanical

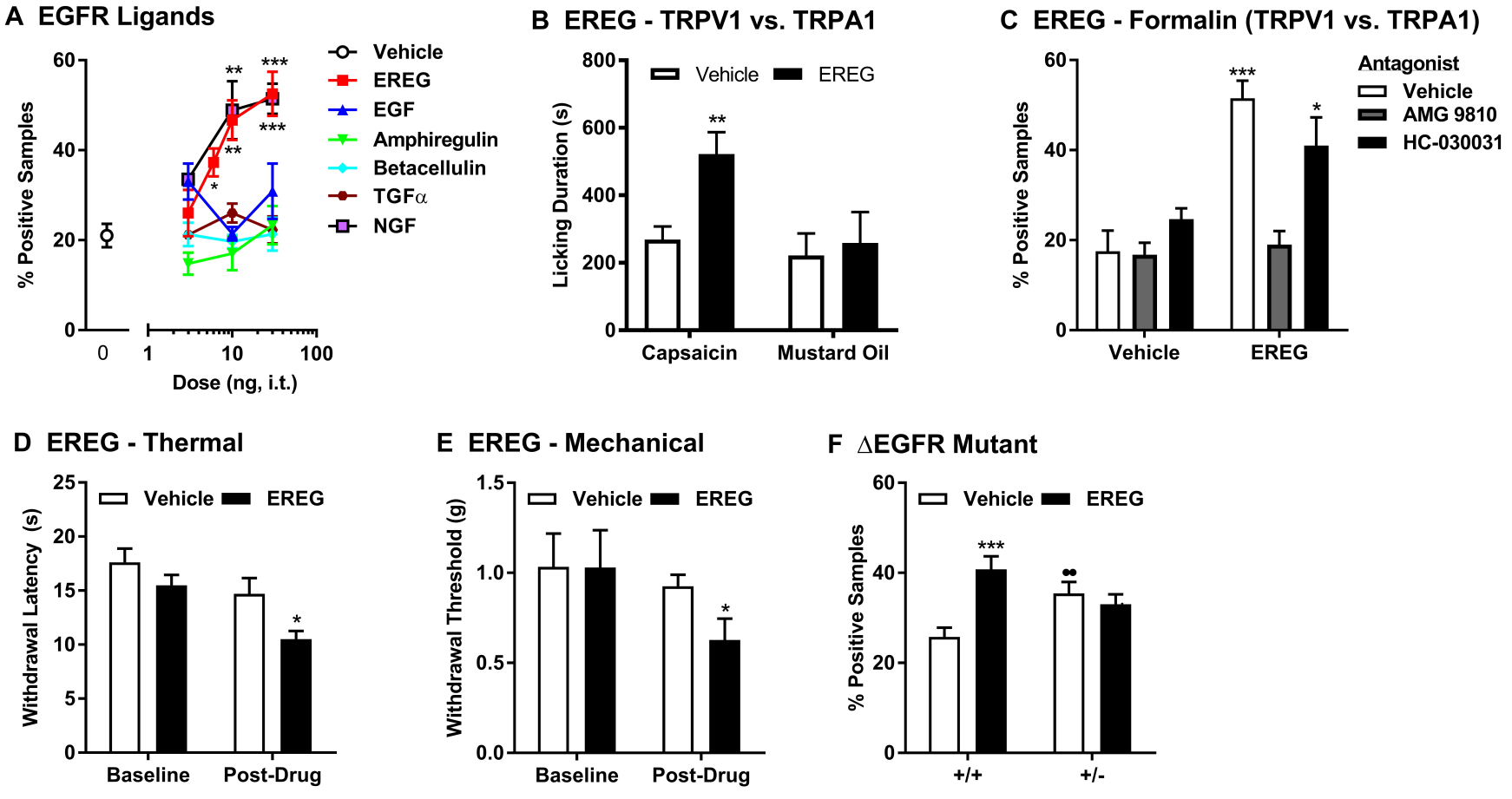
A EGFR Ligands
% Positive Samples
Dose (ng, i.t.)
Vehicle
EREG
EGF
Amphiregulin
Betacellulin
TGFα
NGF
B EREG - TRPV1 vs. TRPA1
Licking Duration (s)
Vehicle
EREG
Capsaicin
Mustard Oil
C EREG - Formalin (TRPV1 vs. TRPA1)
% Positive Samples
Antagonist
Vehicle
AMG 9810
HC-030031
Vehicle
EREG
D EREG - Thermal
Withdrawal Latency (s)
Vehicle
EREG
Baseline
Post-Drug
E EREG - Mechanical
Withdrawal Threshold (g)
Vehicle
EREG
Baseline
Post-Drug
F ΔEGFR Mutant
% Positive Samples
Vehicle
EREG
+/+
+/-

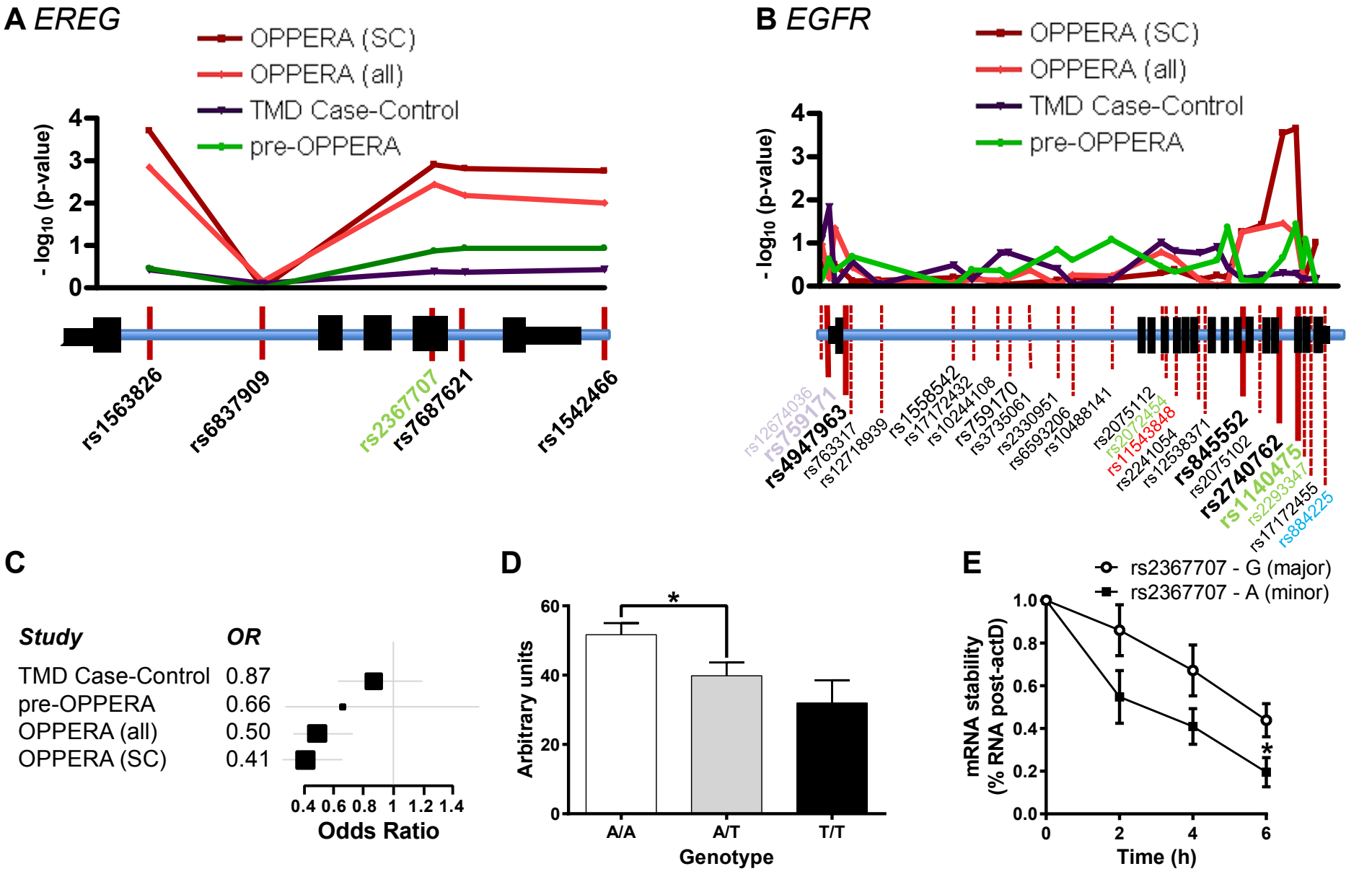
A EREG
OPPERA (SC)
OPPERA (all)
TMD Case-Control
pre-OPPERA
- log10 (p-value)
rs1563826
rs6837909
rs2367707
rs7687621
rs1542466
B EGFR
OPPERA (SC)
OPPERA (all)
TMD Case-Control
pre-OPPERA
- log10 (p-value)
rs12674036
rs759171
rs4947963
rs763317
rs12718939
rs1558542
rs17172432
rs10244108
rs7759170
rs3735061
rs2330951
rs6593206
rs10488141
rs2075112
rs2072454
rs11543848
rs2241054
rs12538371
rs845552
rs2075102
rs2740762
rs1140475
rs2293347
rs17172455
rs884225
C
Study
OR
TMD Case-Control 0.87
pre-OPPERA 0.66
OPPERA (all) 0.50
OPPERA (SC) 0.41
0.4 0.6 0.8 1 1.2 1.4
Odds Ratio
D
Arbitrary units
*
A/A
A/T
T/T
Genotype
E
rs2367707 - G (major)
rs2367707 - A (minor)
mRNA stability
(% RNA post-actD)
*
Time (h)

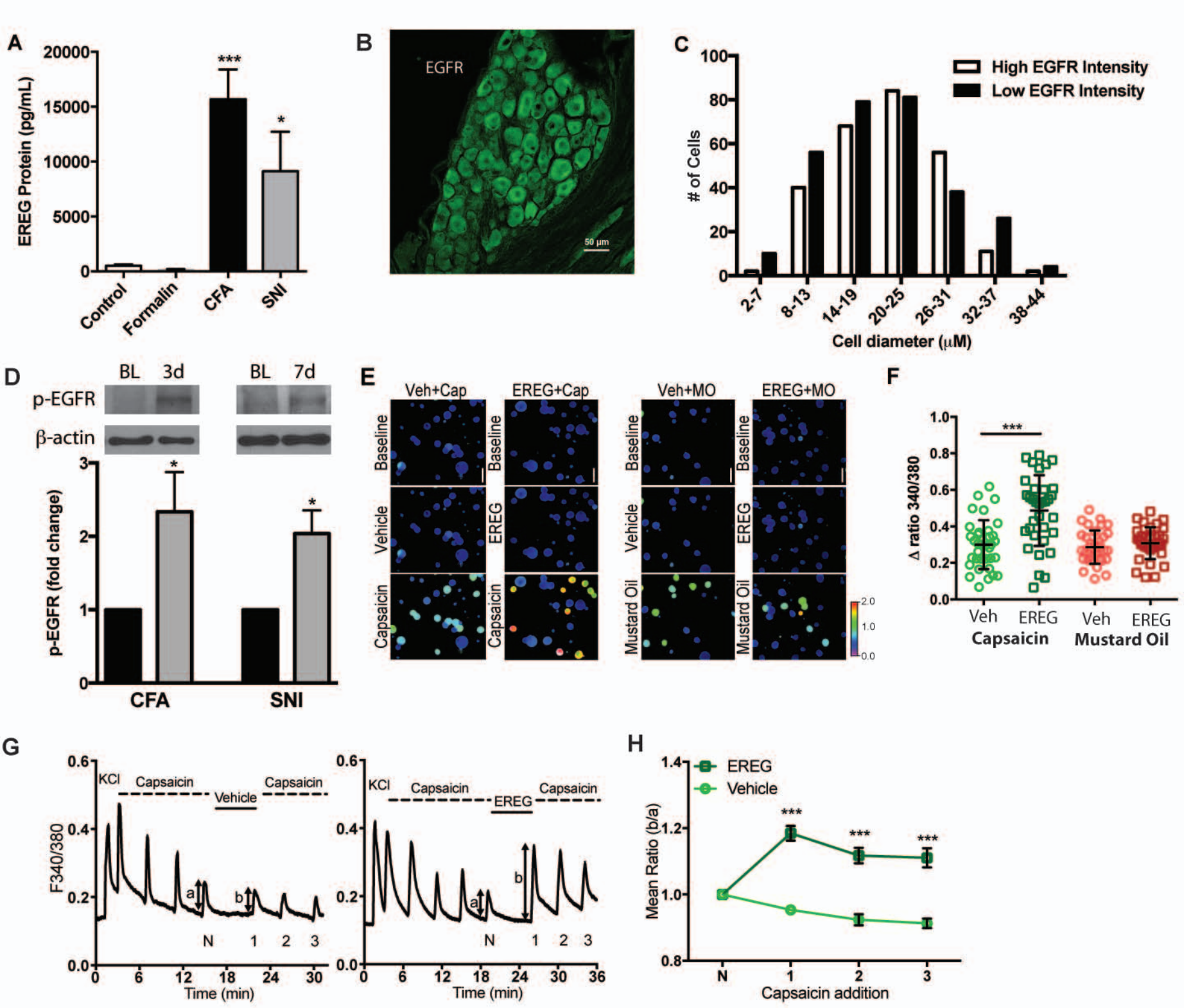
A
EREG Protein (pg/mL)
20000
15000
10000
5000
0
***
*
Control
Formalin
CFA
SNI
B
EGFR
50 µm
C
# of Cells
100
80
60
40
20
0
High EGFR Intensity
Low EGFR Intensity
2-7
8-13
14-19
20-25
26-31
32-37
38-44
Cell diameter (µM)
D
BL
3d
BL
7d
p-EGFR
β-actin
p-EGFR (fold change)
3
2
1
0
*
*
CFA
SNI
E
Veh+Cap
EREG+Cap
Veh+MO
EREG+MO
Baseline
Vehicle
Capsaicin
EREG
Mustard Oil
2.0
1.0
0.0
F
Δ ratio 340/380
1.0
0.8
0.6
0.4
0.2
0.0
***
Veh
EREG
Veh
EREG
Capsaicin
Mustard Oil
G
F340/380
0.6
0.4
0.2
0.0
KCl
Capsaicin
Vehicle
Capsaicin
a
b
N
1
2
3
0
6
12
18
24
30
Time (min)
EREG
36
H
Mean Ratio (b/a)
1.4
1.2
1.0
0.8
EREG
Vehicle
***
***
***
N
1
2
3
Capsaicin addition

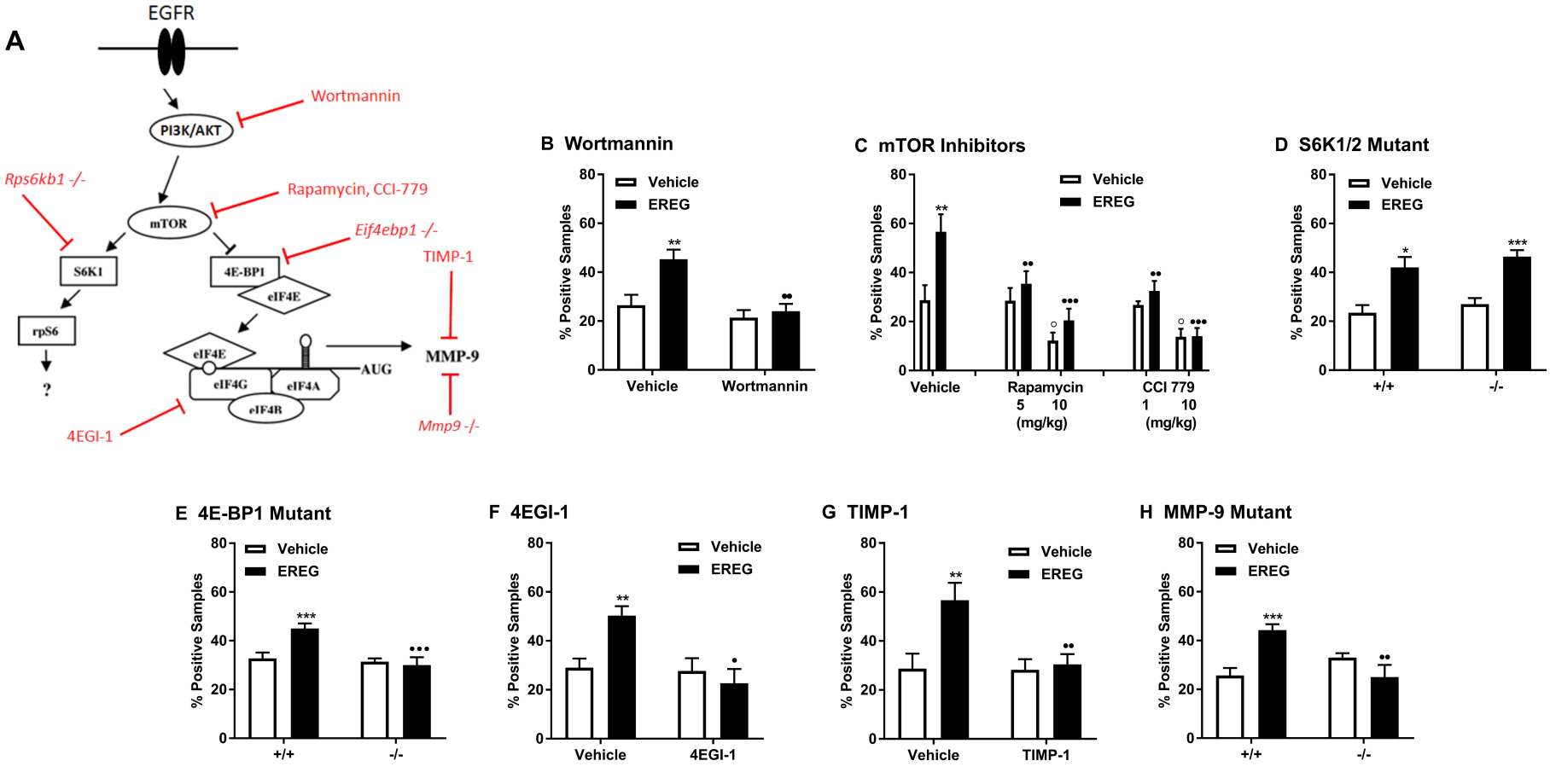
A
EGFR
Wortmannin
PI3K/AKT
Rps6kb1 -/-
Rapamycin, CCI-779
mTOR
Eif4ebp1 -/-
TIMP-1
S6K1
4E-BP1
eIF4E
rpS6
?
eIF4E
AUG
MMP-9
eIF4G
eIF4A
eIF4B
4EGI-1
Mmp9 -/-
B Wortmannin
% Positive Samples
Vehicle
EREG
Vehicle
Wortmannin
C mTOR Inhibitors
Vehicle
Rapamycin
5 10
(mg/kg)
CCI 779
1 10
(mg/kg)
D S6K1/2 Mutant
+/+
-/-
E 4E-BP1 Mutant
F 4EGI-1
4EGI-1
G TIMP-1
TIMP-1
H MMP-9 Mutant